Defining Antarctic polynyas in satellite observations and climate model output to support ecological climate change research

Laura Landrum[1], Alice K. DuVivier[1], Marika M. Holland[1], Kristen Krumhardt[1], Zephyr Sylvester[2]

[1]NSF National Center for Atmospheric Research, Boulder, CO, USA
5 [2]INSTAAR, University of Colorado, Boulder, CO, USA

Correspondence to: Laura Landrum (landrum@ucar.edu)

Abstract. Antarctic polynyas are key components of Antarctic marine ecosystems, influencing light and nutrient availability and open water access for marine predators. Thus, changes in the physical characteristics of polynyas can influence how these ecosystems respond to a changing climate. Here, we explore how to identify polynyas using satellite and Earth System Model

10 data, and we assess the impacts of using different polynya-identification metrics (sea ice concentration or thickness). Our results show optimal metrics for polynya definition will depend on the temporal and spatial resolution of the data, as well as the season and region of interest. These results highlight the importance of identifying polynyas on grids of the same type and resolution when comparing polynyas from different data products. We find that sea ice thickness is more suitable for identifying polynyas in model data in winter months in contrast to spring months when both sea ice thickness and concentration

15 may be suitable metrics. We then use the Community Earth System Model Version 2 (CESM2) to investigate ecosystem function within polynyas and find that there is enhanced phytoplankton productivity in modeled polynya features in both hindcast and fully coupled simulations, with springtime polynyas remaining an important control on Antarctic productivity under future climate change.

1 Introduction

20 Sea ice is an important component of the Antarctic physical Earth system and has a strong influence on ecosystems. Pan-Antarctic sea ice changes have been exceptionally variable in recent years, and regional trends can also differ substantially in sign and magnitude (e.g., Fogt et al., 2023; Parkinson 2019; Purrich & Doddridge, 2023; Raphael & Handcock, 2022; Turner et al., 2017; Turner et al., 2022). Yet, assessing pan-Antarctic or regional ice area trends does not address changes in important Antarctic sea ice features, specifically coastal polynyas. Polynyas are regions of reduced sea ice concentration surrounded by

25 higher sea ice concentrations and/or coastline, and both open water ("sensible heat") and coastal ("latent heat") polynyas are found in the Antarctic sea ice zone. Open water polynyas are created when relatively warm ocean water upwells to the surface thermodynamically melting sea ice. Coastal polynyas are driven by cold downslope winds off the Antarctic continent that mechanically push sea ice away from the coast leaving open water that can rapidly freeze into more sea ice.

30   Coastal polynyas occupy only a small area within the Southern Hemisphere sea ice zone yet play an outsized role in Antarctic sea ice production, deep water formation, global thermohaline circulation, carbon sequestration, and biological activity. As regions of lower sea ice concentration and thinner sea ice, polynyas are the first oceanic regions exposed to light in the Antarctic spring. As a result, polynyas show enhanced production within the Antarctic sea ice zone, where phytoplankton growth tends to be limited by light (Arrigo and van Dijken, 2003) and spring phytoplankton blooms within polynyas are frequently

35   synchronized with light availability (e.g. Li et al., 2016). Polynyas also provide Antarctic predators (e.g., penguins, seals) both open water access and augmented prey resources, with ephemeral polynyas being of particular importance for Emperor penguins (Labrousse et al., 2019).

How Antarctic marine ecosystems respond to a changing climate will be determined, at least in part, by changes in size,

40   location and timing of coastal polynyas. Defining polynyas as areas of relatively open water surrounded by sea ice and/or land, which is a common way to refer to these features, is a subjective definition which does not consider questions of scale and polynya functioning. In order to use climate models to investigate how Antarctic polynyas may change in the future, we need to both assess the impacts of different polynya definitions for gridded data and investigate how polynyas estimated from model output compare with those estimated from satellite images over the historical period. Objective and quantifiable methods to

45   identify polynyas are necessary in order to assess their role in the climate and ecological system, compare observations with model output, and make inferences regarding future polynya change.

Polynyas and polynya-like features often have scales and dimensions much smaller than those resolved by either satellite observations or global climate model data. Furthermore, sea ice concentrations (SICs) are calculated using different products

50   and methodologies in observational data sets and climate model simulations. The long-term (since 1979) record of satellite SIC is based on passive microwave images, whereas model sea ice concentration data are based on the physical evolution of simulated sea ice due to fluxes of energy and momentum. These differing definitions of the same field complicate comparisons of polynyas based on observational and model products. Passive microwave images tend to underestimate SICs at low concentration levels and in thin ice areas (e.g. Meier, Windnagel and Stuart, 2021; Ivanova et al., 2015 and references therein),

55   whereas climate model simulations calculate SICs to very small fractions and sea ice thicknesses (SITs) to very thin thicknesses, albeit with potential biases from forcing or structural model uncertainty. Additionally, satellite-derived SIT estimates remain spatially and temporally limited and have considerable uncertainty compared with SIC products (e.g. Kacimi & Kwok, 2022; Zygmuntowska et al., 2014 and references therein). Thus, SIT from satellite products has limited capacity for identifying thin sea ice which may be relevant for polynyas. In addition, climate model SICs and SITs are calculated at the

60   model time-step (e.g. every hour) then averaged over a day for daily averages, whereas satellite observations of SIC or SIT represent an instantaneous snapshot of conditions (typically daily or bi-daily; Meier et al., 2014) specific to a particular time and location.

Previous studies have identified polynyas using various metrics and methods. In a study investigating the influence of various

65 factors on the formation of polynyas in Eastern Antarctica, Massom et al (1998) found that a SIC threshold of 75% (where any grid cells below 75% SIC were identified as a polynya) worked well with the monthly 25kmX25km gridded passive microwave SICs to differentiate polynyas from the marginal ice zone. Arrigo & van Dijken (2003) used a satellite derived, downscaled (6.25kmX6.25km) passive microwave SIC product and utilized both concentration (10%) and time (>50% of winter days) thresholds to identify wintertime polynyas around the entire continent. The resulting polynya maps were further refined by

70 whether neighboring pixels merged later in the season to form larger "post polynyas". Satellite-derived chlorophyll images (O'Reilly et al., 1998) have also been used to define "polynya regions" within which to further study phytoplankton dynamics, but satellite-based chlorophyll products can only identify polynyas in areas of both open water and clear skies. Tamura et al. (2006) proposed new algorithms for estimating sea ice thicknesses in thin sea ice areas and for differentiating thin sea ice from fast ice in the passive microwave data. The resulting maps of sea ice thicknesses in thin sea ice areas along with reanalysis

75 data from both the European Centre for Medium-Range Weather Forecasts (ERA-40) and the National Centers for Environmental Prediction (NCEP2) were used to make maps of sea ice production and variability in Antarctic polynyas (Tamura et al., 2007; Tamura et al., 2015). This method of identifying thin sea ice areas was applied in work investigating the influence of icescapes on Emperor penguin foraging habitat in East Antarctica (Labrousse et al., 2019). More recently, Mohrman et al. (2021) identified polynyas using gridded SICs and SITs from 27 CMIP6 climate models, as well as the

80 European Organisation for the Exploitation of Meteorological Satellites (EUMETSAT) Ocean and Sea Ice Satellite Application Facility (OSI SAF; Lavergne et al., 2019) satellite observations, to explore differences in open water and coastal polynya formation in climate models. Polynyas were identified by applying a <30% SIC threshold or <12 cm SIT threshold to all data on the respective native grids (which ranged from 25 km to 250 km nominal resolutions; Mohrman et al., 2021). Duffy et al. (2024) applied a <50% SIC definition to daily satellite SIC data on a 25kmX25km grid to define polynya areas. These

85 multiple working definitions of polynyas are not consistent, and to the best of our knowledge, no one has published work showing the implications of different polynya identification metrics applied to different data sources, at different spatial resolution, or over different temporal periods.

Our goal in this work is to explore different methods of defining polynyas based on gridded time series data, to define metrics

90 that are reproducible, verifiable, and useful for assessing polynyas in present and future climate states. We also seek to understand how choice of polynya metrics may influence results in terms of polynya area, frequency, trends and location. We intend for this exploration to give guidance on implications of various polynya metric choices for model and satellite-based data analysis. The role of low sea ice areas in Antarctic marine ecosystems is dynamic and diverse – polynyas affect availability of light and nutrients for phytoplankton, provide open water access and thus prey for marine predators such as penguins and

95 seals, and the timing of low sea ice conditions influences the seasonal progression of phytoplankton blooms. In this paper, we investigate the impacts of metric choices on polynya identification, compare polynya areas estimated from simulated and observed data, assess if our polynya metrics identify biologically important marine regions, and apply these metrics to a large

ensemble of historical and future climate scenarios. This analysis provides comprehensive and quantifiable information on
polynya identification that can be used in future work to assess the role of changing polynyas on Antarctic marine ecosystem
100 dynamics and the physical environment.

2 Data

105 2.1 Satellite observations

The primary observational product we consider is the daily 1979-2020 Climate Data Record (CDR) sea ice concentration
satellite data product available from the National Snow & Ice Data Center (NSIDC; Meier et al., 2014; Meier et al., 2021).
The CDR data are a merged product of the NASA Team and Bootstrap algorithms, with the higher SIC of the two products
used as the CDR value when the two products differ (Meier et al., 2014). We calculate polynya maps for the CDR product on
110 both the original (25 km x 25 km) Equal Area Scaleable Earth (EASE) grid as well as regridded onto a nominal 1° climate
model grid, as described below. The reason to create maps on both grids is to better understand the impact of resolution on the
identification of polynyas in different types of products (i.e. satellite observations and Earth System Models) that span large
spatial scales. Additionally, given the differences in instantaneous satellite observations and model average conditions, we
apply our polynya metrics to daily and monthly averaged data to better understand the impacts of temporal resolution on
115 polynya identification. Finally, satellite data products that use different algorithms for calculating sea ice concentrations from
images can lead to differences across the SIC fields, so we also compare polynya metrics using SICs from the CDR and the
NASA Team products for additional insights.

2.2 Climate Model Output

120 This study uses output from the Community Earth System Model Version 2 (CESM2; Danabasoglu et al. 2020) for climate
model data. We use model output from two different configurations of the CESM2: an ocean-ice hindcast forced by
atmospheric reanalysis data, and a fully-coupled configuration forced by the Coupled Model Intercomparison Project Phase 6
(CMIP6) protocols for the historical (1850-2014) and future (2015-2100) high emissions scenario (SSP370; Eyring et al.,
2016). Both CESM2 configurations are on the standard nominal 1° grid. The JRA-CESM hindcast simulation (Krumhardt
125 al., 2024) is a prognostic ice-ocean simulation with CESM2 that is forced by the Japanese Reanalysis product (JRA-CESM;
Kobayashi et al., 2015; Tsujino et al., 2018) for atmospheric conditions. The fully coupled simulations (Danabasoglu et al.,
2020) use a standard configuration that was a contribution to CMIP6 (Eyring et al., 2016) and have fully prognostic

atmosphere, ocean, sea ice, and land components. We also show results from 50-members of the CESM2 Large Ensemble that use standard CMIP6 forcing (CESM2-LE; Rodgers et al., 2021).

130

For ocean biogeochemistry, both CESM2 configurations were run with the Marine Biogeochemical Library (MARBL) model (Long et al., 2021), which simulates planktonic marine ecosystem dynamics and coupled cycles of carbon, nitrogen, phosphorus, iron, silica, and oxygen. MARBL is highly configurable, allowing a flexible number of plankton functional types. In this study, the fully coupled simulation uses the planktonic MARBL ecosystem described in Long et al (2021), while JRA-

135 CESM uses a slightly more complex ecosystem, described in Krumhardt et al. (2024). We focus on net primary productivity (NPP) here, which is the sum of net carbon fixation by all phytoplankton functional types. All configurations of CESM simulations compute light penetration based on a subgrid-scale sea ice thickness, important for capturing the non-linear photosynthetic function in ice-covered waters (Long et al., 2015).

140 The JRA-CESM represents the closest simulation to the observed satellite record and thus we use this simulation for the bulk of our model-satellite polynya comparisons. Antarctic SIC and sea ice extents (SIE; defined as the area covered by sea ice concentrations of 15% or higher) in the JRA-CESM compare well, spatially and temporally (Krumhardt et al., 2024), with the NSIDC Climate Data Record (CDR; Meier et al., 2021) and the NSIDC Sea Ice Index (Fetterer et al., 2017). The sea ice component of the CESM2 used in all configurations shown here includes a "mushy" thermodynamic component that allows

145 for a mixture of brine and solid ice and and leads to increase in both frazil ice production and Antarctic Bottom Water formation in polynya-like coastal features when compared with the CESM1 earlier model version (DuVivier et al., 2021; Singh et al., 2020). This paper presents a more in-depth view of polynyas in the CESM2.

3 Methods

3.1 Polynya algorithm

150 Our algorithm defines polynyas from a particular variable and threshold value. The two physical sea ice variables we focus on for polynya identification are SIC and SIT. Polynyas are identified as contiguous regions of grid cells that fall below a given threshold and are surrounded by land or ice-covered regions above the threshold (e.g. Appendix A). The first step in the algorithm identifies all grid cells that fall below the variable threshold and lie within the ice zone (i.e. not immediately bordering open ocean). In subsequent iterations, the algorithm checks neighboring grid cells. If all grid cells bordering a region

155 of ice below the threshold are bounded by higher threshold variables and/or land, then this region is identified as a polynya. If any neighboring cells are bounded by open ocean, the grid cells are not considered a polynya even though they meet the threshold requirement. This iterative process is necessary in some regions and seasons when the northern ice edge may be complicated as polynyas open up and merge with open water (e.g. in the Ross Sea in austral spring and around the Western Antarctic Peninsula with a relatively complicated coastline). The polynya algorithm also numbers individual polynyas and

160   calculates polynya areas based on the number of grid cells each individual polynya occupies. In this manner, we can calculate not only total polynya area by region, but also the number of individual polynyas and their sizes. This threshold-based algorithm is similar to the method employed by Mohrman et al. (2023), but we identify polynyas for a range of threshold values for satellite-based SICs and model-based SICs and SITs. Our algorithm maps both open-water (surrounded by higher concentrations or thicknesses of sea ice) and coastal (at least one grid-cell neighboring land) polynyas, but this work focuses

165   primarily on coastal polynyas because of their important ecological functions and because open ocean polynyas are relatively uncommon in observations and in the model results.

We first explore the influence of polynya metrics on polynya identification in the satellite and JRA-CESM data by calculating integrated total polynya areas by different time periods (seasonal, annual, monthly) and region (Southern Hemisphere and

170   smaller regions using the regional definitions of Parkinson & Cavalieri, 2012 and shown in Fig. 1f). We then choose one SIC and one SIT polynya threshold metric to apply to the 50-member CESM2-LE. These thresholds are based on the analysis of the integrated polynya areas from the satellite product and the JRA-CESM simulation compared with published estimates of Antarctic coastal polynya areas.

3.2 Impacts of metric thresholds, spatial and temporal resolutions on polynya identification

175   We apply a range of SIC (15%-85%) and SIT (10-85 cm) thresholds to identify polynyas in the CDR satellite product and the JRA-CESM on different spatial and temporal resolutions. Polynyas often have scales and dimensions much smaller than that resolved by standard gridded sea ice data, even the relatively fine resolution CDR data on a $25\mathrm{km}^2$ grid. Thus, appropriate threshold values for identifying polynyas may depend on the size of the data grid cell. As a simplified example, a polynya defined by a 10% SIC threshold on a 6.25 km EASE grid (e.g. the sub-pixel grid used by Arrigo & VanDijken, 2003) and

180   surrounded by grid cells of 100% SIC would be classified as a polynya on 25/45 km EASE grids at 94/98% SIC thresholds (e.g. Appendix B). Polynya threshold choices are further complicated by climate model grids that tend to be in degrees latitude/longitude and are thus not equal-area grids. A given SIC threshold for the equal area grid is the equivalent of an area threshold (i.e. km^2 of open water within a grid cell), whereas on the equal-latitude/longitude grid a given SIC will correspond to different total open water areas within a grid cell depending on latitude (since the grid cell surface area is latitude-dependent,

185   and thus a percentage of the total grid cell area will represent a different area depending on latitude; see Appendix B). Given these considerations and the scientific question at hand, the threshold used may need to depend on grid size and may be specific to region, season, and variable. We explore the impacts of grid size on polynya areas by making polynya maps from different grid sizes in the satellite data – the original 25 km EASE grid and regridded to the standard nominal 1° CESM grid. We compare polynya metrics between satellite and climate model output by focusing on the regridded satellite data.

190

Polynya-like features can change rapidly in time, particularly for wintertime Antarctic coastal polynyas when surface air temperatures are extremely cold and extensive (albeit thin) sea ice can form rapidly at open water surfaces. Polynyas identified

from daily data, for example, may not appear on monthly time scales (particularly in the model, which can simulate high concentrations of very thin sea ice). We investigate the effects of temporal resolution on polynya identification by comparing

195   polynyas estimated from daily and monthly data in both the satellite product and the model output.

3.3 Impacts of differing methodologies for calculating sea ice concentrations in the model and satellite images

Comparing polynya estimates in models and satellite observations is not a trivial matter. Passive microwave images struggle to detect sea ice when concentrations fall below ~10%. As a result, the National Snow & Ice Data Center (NSIDC) Climate Data Record (CDR) implements a 10% minimum threshold on the CDR data product (Meier, Windnagel and Stuart, 2021).

200   Satellite-based SICs are underrepresented in areas of thin sea ice – passive microwave images require SITs greater than ~5 cm to register, and ice between 5 and 20 cm thick will result in systematically underestimated SICs (Ivanova et al., 2015; Walt Meier, personal communication). In contrast, climate model simulations calculate SICs to very small fractions independent of mean SIT. This complicates how a polynya is identified in each dataset. For example, winter-time polynyas can be regions of extremely high sea ice production where sea ice forms nearly as fast as winds expose water to the overlying atmosphere. In

205   these conditions, one might expect polynya metrics based on SIT would be more appropriate than SIC in model output as the extreme cold wintertime air temperatures can lead to nearly immediate sea ice formation and thus high SICs even if SITs are very thin. Conversely, SICs are underestimated in satellite products when the ice is very thin, so a satellite observation in these conditions should show lower SIC (note that observations of SIT are very limited). This is a clear example where SICs may be better suited for defining wintertime polynyas from satellite images whereas SITs might be a better metric from climate

210   model output.

Given the challenges of passive microwave sea ice detection in low ice concentration and thickness conditions, as detailed above, we explore the influence of different definitions for SIC in satellite-based observations and model output by degrading the JRA-CESM hindcast sea ice concentrations such that the modified SICs are more closely aligned with SICs as they would

215   be remotely sensed. Model SICs are degraded by setting daily SIC in grid cells with less than 10% SIC or less than 5 cm daily SIT to 0% SIC, matching the values that a satellite would observe in these conditions. Daily SICs within grid cells that have SITs of 5-20 cm thick are set to half of the original model SIC output, which corresponds to the underestimation of ice concentration over thin ice by satellites (Appendix C). Although using daily averaged data is not the same as the instantaneous satellite-snapshot data, it is the highest frequency model output of sea ice data available. We compare the degraded model SIC

220   to the original output to gain insight into how differences in SIC methodologies may impact polynya identification in both observed and model data products.

3.4 Influence of metrics and resolutions on polynya identification

One of our primary goals in this work is to better understand how different metric choices on a variety of gridded data products will influence polynya identification, and how to best compare polynyas identified in both observational and simulated data.

225   We explore both the influence of resolutions (temporal and spatial grid size) and metric thresholds. We identify polynyas over
a range of SIC thresholds (15%-85%) throughout the year in the satellite based observations on the original EASE grid,
regridded to the nominal 1° model grid, and on both daily and monthly-averaged data. Similarly, we apply the same range of
SIC thresholds as well as a range of SIT thresholds (10-85 cm) to the daily and monthly JRA-CESM. We analyze these results
by month and on both regional and hemispheric scales to elucidate how the influence of polynya identification metric choice
230   may differ by time of year and region.

Based on the analysis of the CDR and JRA-CESM, we pick two polynya identification metrics (85% SIC and 0.4 cm SIT
thresholds on monthly averaged sea ice data) to apply to the 50-member CESM2 over the historical (1850-2014) and future
scenario (2015-2100) time periods. These polynya time series serve as the basis for our exploration of changes in both polynyas
and NPP within polynyas in the future climate.

3.5 NPP and polynyas

Polynyas play important roles in physical and biological processes, and optimal metrics for defining polynyas may differ
depending on analytical goals. Here we explore what constitutes an optimal model-derived polynya metric based on their
ecosystem-relevance, specifically their relation to NPP. During the austral spring (September-October-November), sea ice is
melting and directly impacting NPP through light availability. During this season the optimal choice of metric (SIT or SIC) to
240   define polynyas is not clear, and as such we pick one metric based on SIC and another on SIT to identify polynyas and
investigate if these springtime polynya areas have increased productivity in the JRA-CESM model simulations by calculating
NPP both within the polynya areas and within the sea ice zone (SIZ) as a whole. The SIZ is defined as the region south of the
mean wintertime (June-July-August) northern pack ice (SIC ≧ 85%) boundary. Thus, regions within the ice pack and near the
coast that may have lower sea ice concentrations (e.g. polynyas) lie within the SIZ. The goal is to help inform choices in future
245   studies particularly when using model output that may not include marine biology components or that do not allow for trophic
transfers to higher trophic levels as is critical for high latitude, light-limited systems.

3.6 Polynyas and NPP in a changing climate

In this section we explore how both polynyas and NPP change from the historical time period into the future under the SSP3-
7.0 emissions scenario. We compare results from the CESM2-LE during the historical period with results from the JRA-CESM
250   and the CDR satellite record. We calculate integrated hemispheric NPP both within the SIZ and within springtime polynyas in
the CESM2-LE, comparing both timeseries throughout the historical and future scenarios, and the climate mean annual cycle
of NPP at the beginning (2001-2020) and end (2081-2100) of the 21st Century. We leave analysis of how future changes in
NPP may be related to changes in trophic transfer and phytoplankton function types to future work.

4 Results

4.1 Large-scale sea ice properties

The JRA-CESM and the CESM2-LE generally capture observed Southern Hemisphere (SH) sea ice area means as well as temporal and spatial variability quite well compared to CMIP6 models (e.g. Roach et al., 2020). Both versions of the model underestimate total SH sea ice extent (SIE) from July through October by 10-14% compared with the CDR (Fig. 1e). Regionally, they both tend to underestimate Antarctic sea ice in the Weddell Sea for all months of the year and in Eastern Antarctica in the winter through spring months (Fig. 1 and Supplemental Fig. 1). The largest differences between the JRA-CESM and fully coupled CESM2-LE datasets are also in the Weddell sea and eastern Antarctica. During the austral summer, where both model simulations underpredict sea ice in the Weddell Sea, the CESM2-LE has substantially more sea ice than the JRA-CESM. From winter through spring, the CESM2-LE underestimates sea ice in eastern Antarctica compared with the CDR, however the JRA-CESM simulates more sea ice than the CESM2-LE particularly during the winter. The CESM2 simulations represent a reasonable selection of climate model for identifying Antarctic polynyas because both JRA-CESM and CESM2-LE fully coupled configurations capture the mean climatology of Antarctic sea ice, particularly compared with CMIP6 models (Roach et al., 2020) and simulate coastal polynya-like areas of high sea ice production (Singh et al., 2020; DuVivier et al. 2021).

1979-2020 Mean Sea Ice Extent
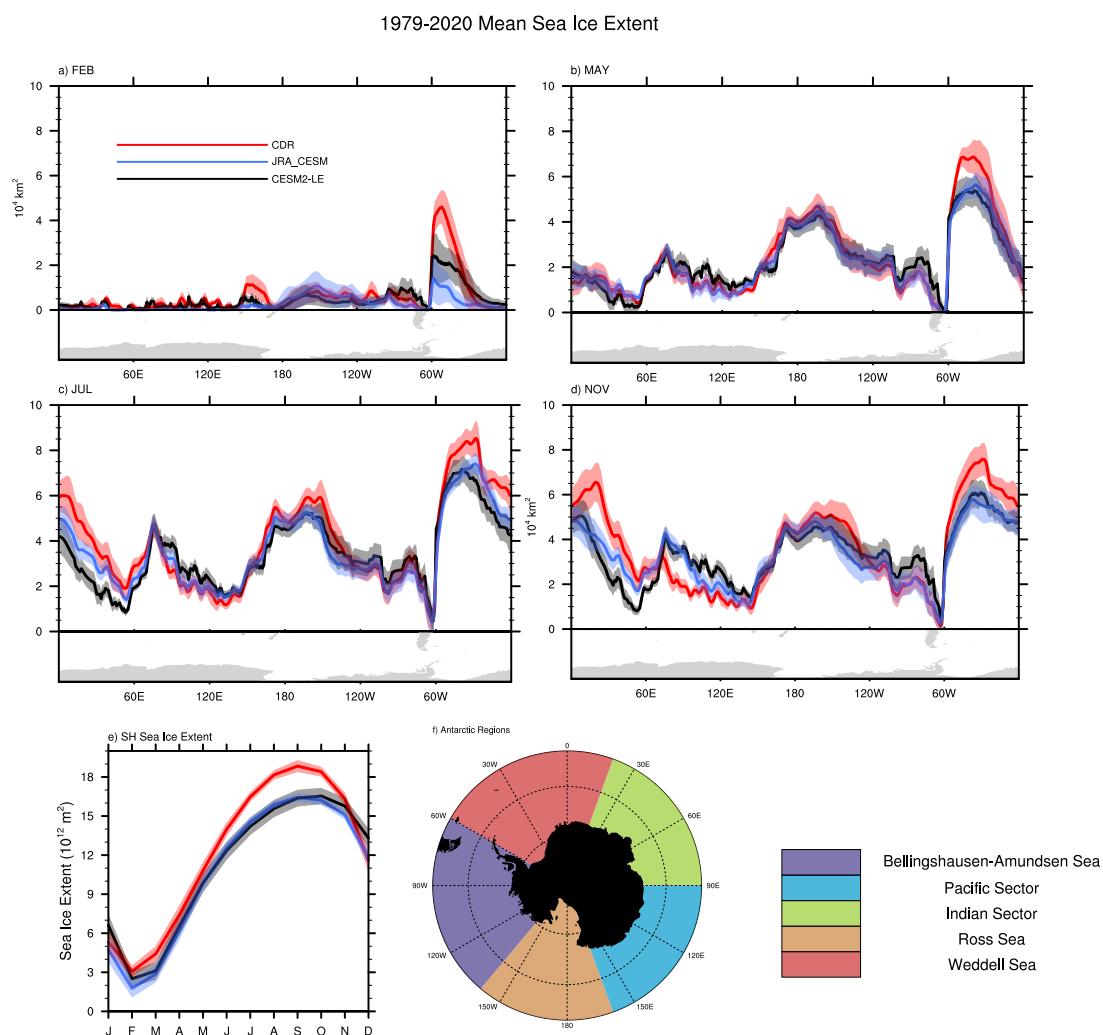
Figure 1. 1979-2020 Monthly mean total sea ice extent as a function of longitude for a) February, b) May, c) July, d) November; e) monthly Southern Hemisphere (SH) Sea Ice Extent (SIE) climatology for the CDR (red), JRA-CESM (blue) and CESM2-LE data; and f) Antarctic regions map. Thick solid line indicates the mean (or ensemble mean for the CESM2-LE), shaded polygon indicates the mean ±1 standard deviation. Sea ice extents as a function of longitude have been smoothed by a 3-point running average.

4.2 Polynyas in the satellite data

Maps of open water and coastal polynyas on July 15, 2003, calculated using our algorithm and a SIC threshold of 85% for observational datasets are shown in Fig. 2 (a-c). Note that this date is not special, but a representative day shown to illustrate differences in polynya identification metrics across products. We picked a random winter day as relatively few polynyas are identified in January-April in all data products (Supplemental Figs. 2-3), polynya area variabilities increase substantially for

10

all metrics in November-December, and the broad similarities and differences between polynyas identified in different data
280 products on this winter day are typical.
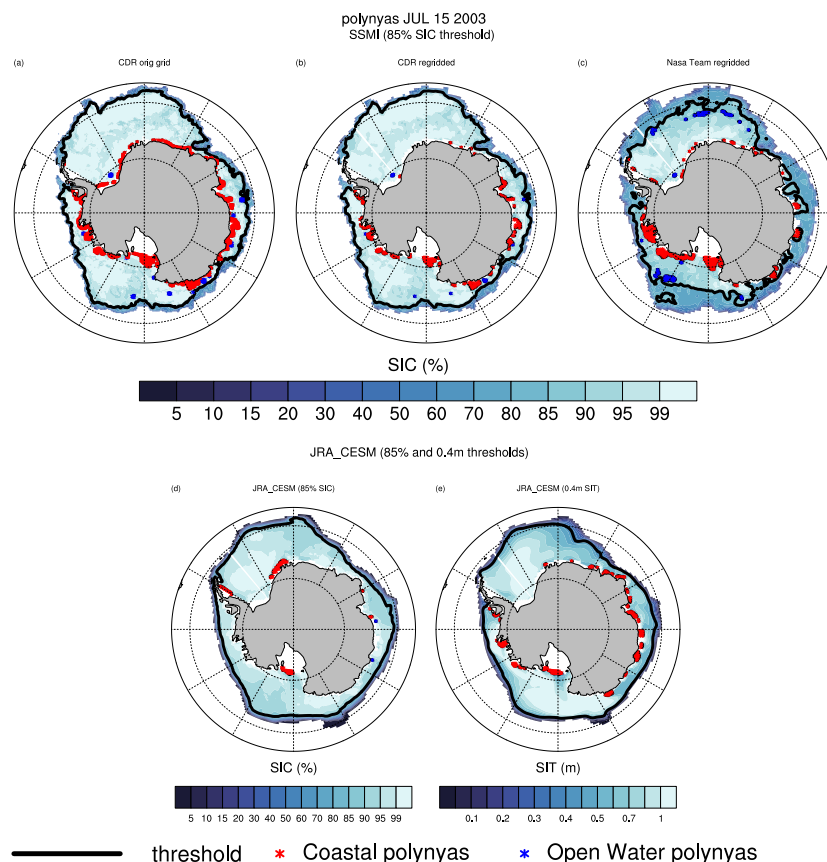
Figure 2. Polynya maps for July 16, 2003 using SIC 85% threshold and the CDR data on the original Equal Area Scaleable Earth
(EASE) grid (a), the CDR regridded to the CESM grid (b), the NASA Team SIC product regridded to the CESM grid (c), the JRA-
CESM (d) and the JRA-CESM using a 0.4m SIT threshold (e). Open water/coastal polynyas are indicated by the blue/red *s. The
285 **85% SIC and 0.4m contours are indicated by the thick black contours over the color-contoured SIC or SIT values. Sea ice
concentrations below 15% are masked out.**

The sea ice edge (defined as the 15% SIC contour) is nearly identical for the three satellite products - CDR on the original
grid, the CDR regridded to the nominal 1° climate model grid, and the NASA Team satellite product - even though the edge
290 of the pack ice (defined as 85% or higher SIC) is much further away from the sea ice edge in the NASA Team product (Fig.
2a-c). As expected based on the discussion of grid size and thresholds (Appendix C), more polynyas are identified using the
same threshold (85% SIC) on the finer grid-resolution CDR than on the regridded, coarser CDR data (Figs. 2 and 3, a-b).
Comparisons of regridded CDR and regridded NASA Team data show that more polynyas and larger area polynyas are
identified using the satellite SICs based on the NASA Team algorithm (Fig. 2 b-c). This is likely because the NASA Team

11

295 algorithm tends to underestimate SICs, particularly during the melt season (Comiso et al., 1997; Meier, 2005). In general, NASA Team SICs are often lower than those of the CDR and result in a larger number of polynyas identified for a given threshold SIC when the products are on identical grids. The regridded NASA Team data also show far more open water polynyas using the 85% threshold than either of the CDR data (regridded or not; Fig. 2a-c).

SH coastal polynya area (1979-2020)
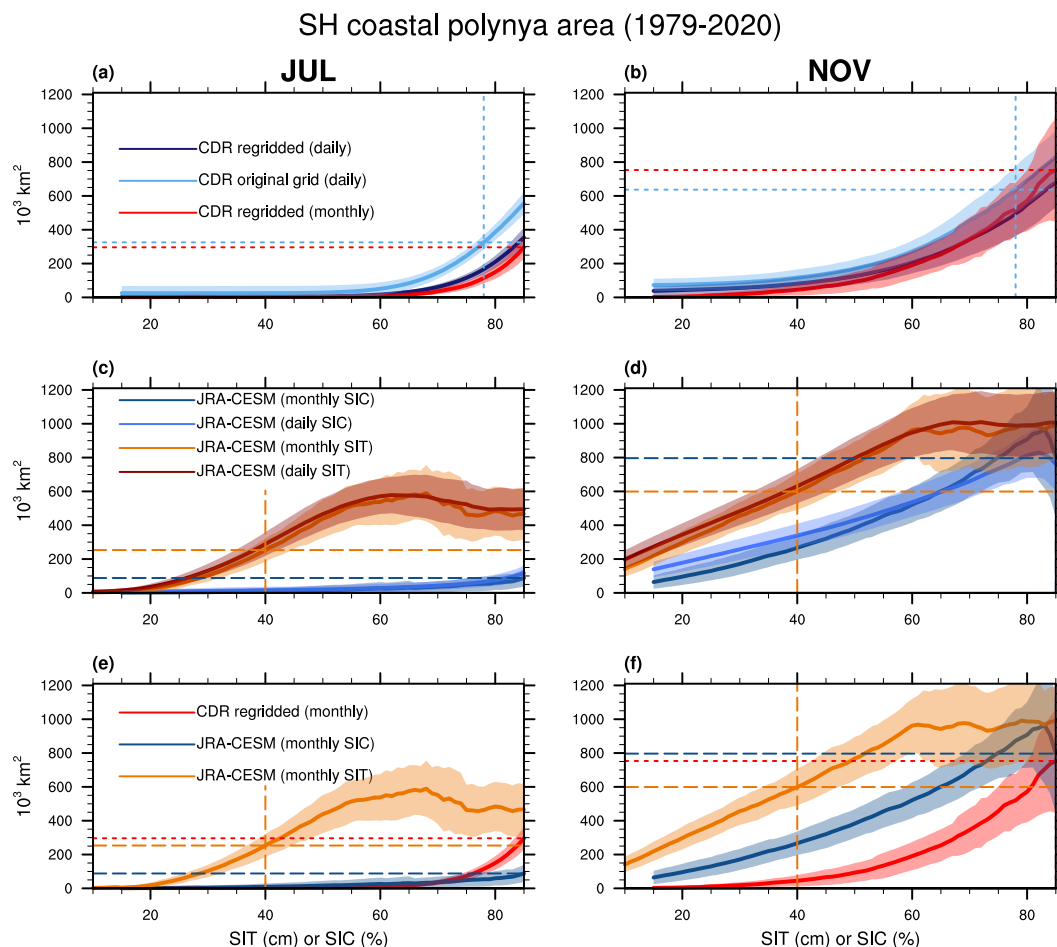
300 **Figure 3. Total SH coastal polynya area as a function of SIC threshold for July (left column) and November (right column) for CDR (top; a-b), JRA-CESM (middle, c-d) and both CDR and JRA-CESM monthly (e-f). Colors correspond to CDR data: daily original EASE grid (dark blue), data data regridded to the CESM grid (light blue), and monthly averaged regridded data (red); JRA-CESM: monthly SIC (dark teal), daily SIC (blue), monthly SIT (orange) and daily SIT (brown). Climatological mean (1979-2020) values are shown in the thick lines; ±1 standard deviations shown by the lighter shading. The dashed lines indicate mean polynya areas at 78%**
305 **SIC in the CDR original grid (light blue), 85% SIC in monthly regridded CDR (red), and 85% SIC (dark teal), and 0.4m SIT (orange) in the monthly JRA-CESM.**

When moving beyond an example day and looking across all years, there are significant differences in integrated total SH area of coastal polynyas in the satellite-based data products as identified by SIC threshold value, grid resolution, temporal resolution

310 (daily vs monthly) and season (Fig. 3 a-b and Supplemental Fig. 2). The total area of coastal polynyas is larger for a given threshold in the CDR on the original higher-resolution EASE grid than when regridded to the 1° CESM grid, and these differences are most pronounced from late fall through early spring (May-Oct; Supplemental Fig. 2). In general, polynyas identified using daily data lead to larger total polynya area April through October across the SIC thresholds than those based on monthly data, and the mean integrated polynya areas based on the daily data often lie more than one standard deviation

315 higher than those based on the monthly mean data. As spring turns to summer, the sensitivity of polynya area to threshold value becomes larger than any differences in the means calculated from different grid and temporal resolutions (Fig. 3b and Supplemental Fig. 2). Throughout most of the year, differences due to temporal resolution are much smaller at a given SIC threshold than the differences due to grid-size. That is, more grid cells are identified as polynyas, and the total SH polynya area is larger on the original, finer-grid EASE grid than on the regridded data for a given threshold value.

320

SH annual mean polynya area as a function of threshold suggests that, on average, for a given SIC threshold the polynya area for the daily regridded data is lower than for the daily data on the original grid (Fig. 3a, b). We pick a SIC threshold value of 85% for the regridded, monthly CDR data both for illustrative purposes and because this threshold results in a total 1979-2020 climatological SH polynya areas similar to those estimated from observations in other studies (e.g. Arrigo & Van Dijken, 2003;

325 Tamura et al., 2008; Nihashi & Ohshima, 2015). Similar SH polynya areas are identified in the daily CDR on the original EASE grid by using a 78% SIC threshold - a value ~7% lower than that used on the CDR data on the 1° model grid.
There are monthly differences in this offset in threshold where the polynya areas from the daily CDR on the EASE grid result in slightly larger or smaller areas than those using an 85% SIC threshold on the daily regridded data (Fig. 3a-b; Table 1, and Supplemental Fig. 2). Even though the magnitudes of SH polynya areas identified in the CDR on the original EASE grid and

330 the 1° model grid are similar, the number of polynyas identified in the CDR on the EASE grid is roughly twice as large as the number identified on the 1° model grid (Table 1), underscoring yet another complication when comparing polynyas estimated from different grid sizes (e.g. Appendix B).

1979-2020 SH coastal polynya mean area, mean number, and trends

	Data, threshold	July	November	ANN
polynya area (10^3 km^2)	JRA-CESM 85% SIC	88 (51)	797 (349)	201 (35)
	JRA-CESM 0.4m SIT	253 (68)	599 (108)	297 (43)
	CDR 85% SIC	296 (66)	753 (307)	275 (31)
	CDR EASE grid 78% SIC	326 (44)	637 (138)	308 (28)
# polynyas	JRA-CESM 85% SIC	8.5 (2.9)	27 (6)	9 (1)
	JRA-CESM 0.4m SIT	21 (4.6)	22 (4)	15 (1.3)

	CDR 85% SIC	42 (5.3)	34 (5.8)	29 (2.6)
	CDR EASE grid 78% SIC	83 (15.4)	64 (14)	57 (12.4)
Mean polynya size (10³ km²)	JRA-CESM 85% SIC	10.4	30.0	21.4
	JRA-CESM 0.4m SIT	12.0	27.6	19.9
	CDR 85% SIC	7.0	22.3	9.6
	CDR EASE grid 78% SIC	3.9	10.0	5.4
Polynya area trends (10³ km²/decade)	JRA-CESM 85% SIC	-2.4	-68.2	**-9.5**
	JRA-CESM 0.4m SIT	**-21.4**	-15.4	**-10**
	CDR 85% SIC	**-15.1**	3.8	-6.6
	CDR EASE grid 78% SIC	**-13.3**	**-35.6**	-5.9
# polynya trend (#/decade)	JRA-CESM 85% SIC	0	-0.1	0
	JRA-CESM 0.4m SIT	0	**0.1**	**0.5**
	CDR 85% SIC	-0.1	0.1	**-0.9**
	CDR EASE grid 78% SIC	**-7.0**	**-6.4**	**-4.5**

Table 1. Climatological polynya area mean (and standard deviation), number of polynyas mean (and standard deviation), average polynya size and Theil-Sen non-parametric linear trend in total polynya area and number of polynyas for polynyas identified on the CESM nominal 1° grid and monthly data. Bold text indicates trends that are at 95% or higher significance based on the Mann-Kendall non-parametric trend significance (Mann 1945, Kendall 1975, Gilbert 1987).

Maps of climatological, coastal polynya areas as a function of longitude from the CDR data are highly correlated for all months across geographic (EASE, regridded) and temporal resolutions (daily and monthly), suggesting that the primary differences are in the magnitude of polynya area rather than regional variability (Fig. 4). There are, however, some regional exceptions. For example, polynya areas estimated using regridded CDR data at an 85% SIC threshold tend to be larger from estimations using the daily data than those using the monthly data in all regions except in the Ross Sea in November, where the opposite is true (Fig. 4). November sea ice is both highly variable and rapidly retreating (Fig. 1e), and the Ross Sea polynya often merges with the open ocean during November (not shown) – polynya areas identified using daily data can become "open water" overnight and the daily polynya area will suddenly drop, whereas the monthly averages may capture, on average, a higher polynya area due to smoother seasonal transitions of the ice pack. Additionally, polynya areas tend to be 46-78% (34-70%) higher (lower) in the Ross and Weddell Seas in July (November) in the CDR on the EASE grid (78% SIC threshold) than the CDR on the 1° model grid (85% SIC threshold). Polynya areas estimated from the CDR on the two different grids tend to be more comparable in the Bellingshausen-Amundsen Sea and Indian Sector.
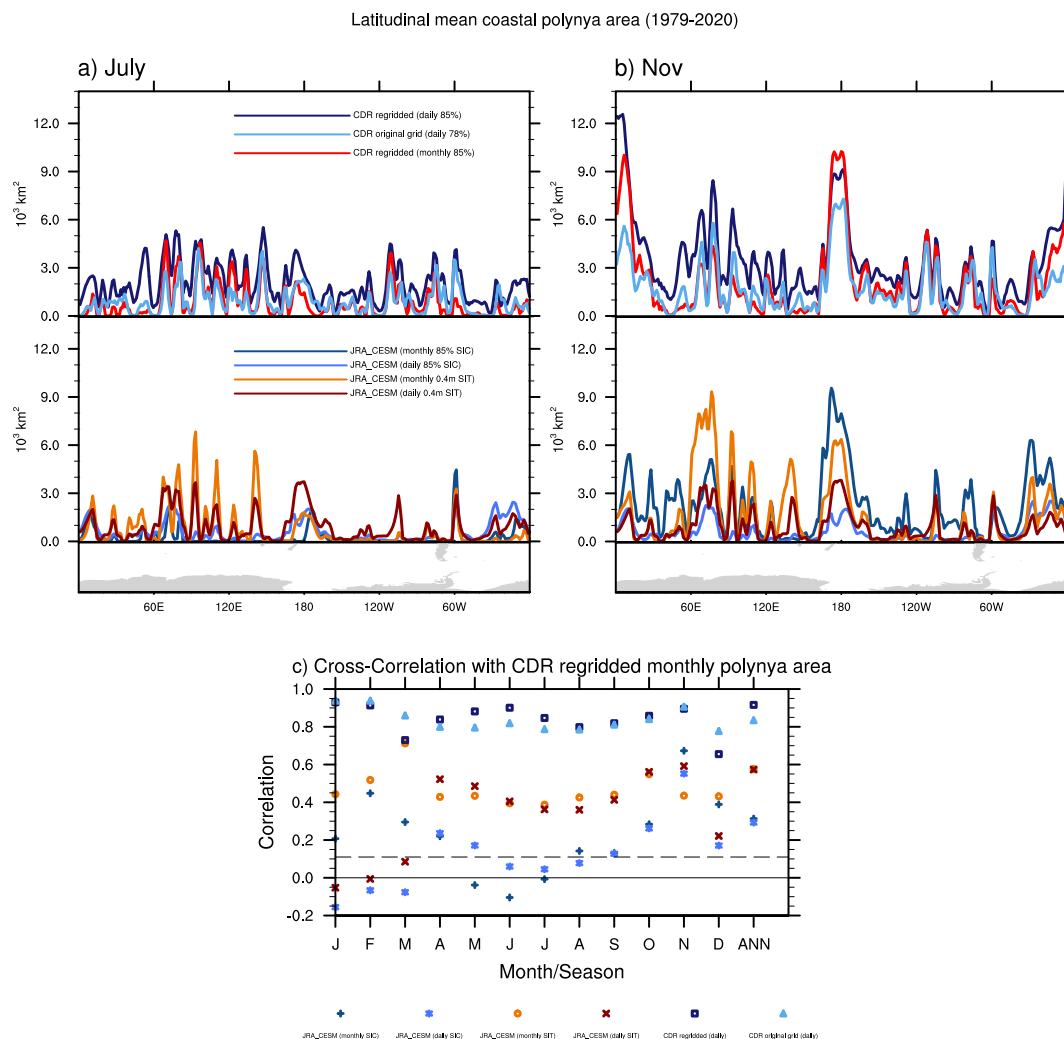
Figure 4. Monthly mean coastal polynya area as a function of longitude for a) July, b) November and c) cross-correlations between monthly averaged coastal polynya area as a function of longitude with those calculated using the regridded CDR monthly data.
355 **Polynya area as a function of longitude is shown as a 3° (longitudinal) running average. Top panels in a) and b) show polynya areas for three different observationally based SICs and polynya thresholds – daily SSMI CDR data regridded onto the CESM grid (red; 85% SIC) and on the original EASE 25km² grid (light blue; 78% SIC), and CDR monthly data on the CESM grid (dark blue; 85% SIC). Bottom panels in a) and b) show polynya areas based on JRA-CESM model simulation using different polynya thresholds: monthly (dark teal) and daily (blue) SIC at 85% threshold, and monthly (orange) and daily (brown) SIT at 0.4m threshold. Cross**
360 **correlations are calculated for polynya areas identified from the monthly CDR regridded data and polynya areas identified in the daily, original-EASE grid CDR (light blue triangles), the daily regridded CDR (dark blue squares), the monthly JRA-CESM SIT (orange circles), the daily JRA-CESM SIC (blue stars), and the monthly JRA-CESM SIC (teal plus signs). The dashed line in c) indicates the 95% significance level.**

15

Curiously, integrated SH polynya areas estimated using the CDR on the original grid have significant negative trends in
365 November, however not in the regridded product (monthly - shown in Table 1 - or daily, not shown). Regional polynya areas
estimated from the CDR on both grids show significant negative trends in July in the Weddell Sea and in July and annually in
the Bellingshausen-Amundsen Sea (Table 2). The only significantly positive trends are found in the Pacific sector on an annual
basis (on both grids). Thus, polynya areas identified in the CDR on the equal area grid and on the equal lat/lon grid lead to
different trend results (although not contradictory as the trends are not significant). This highlights how data on different grids
370 can result in different areas of polynyas seasonally and regionally, and resulting both from different grid resolutions as well as
different types of grids, as discussed above and shown in Appendix B.

Coastal polynya area (10^3 km^2) and trends (10^3 km^2/decade)

Region	Data, threshold	July		November		Annual	
		Area (std)	Trend	Area (std)	Trend	Area (std)	Trend
Ross	JRA-CESM 85% SIC	17 (11)	-1.5	234 (144)	9.7	42 (14)	0.3
	JRA-CESM 0.4m SIT	30 (19)	-2.5	128 (43)	-3.5	75 (31)	-2.8
	CDR 85% SIC	41 (17)	-3.8	232 (88)	-10.4	58 (21)	-3.3
	CDR EASE grid 78% SIC	60 (12)	**-3.7**	168 (47)	**-17.0**	72 (15)	**-3.4**
Bellingshausen-Amundsen	JRA-CESM 85% SIC	1 (2)	0	99 (66)	0.5	12 (6)	-0.2
	JRA-CESM 0.4m SIT	9 (15)	0	26 (24)	2.6	33 (15)	0.7
	CDR 85% SIC	68 (39)	**-15.7**	116 (45)	8.2	64 (21)	**-8.7**
	CDR EASE grid 78% SIC	70 (23)	**-11.8**	111 (30)	4.8	73 (16)	**-7.2**
Weddell	JRA-CESM 85% SIC	49 (42)	4	225 (223)	-30	87 (23)	-4.3
	JRA-CESM 0.4m SIT	33 (24)	-4.3	120 (63)	-14.3	62 (21)	-4.8
	CDR 85% SIC	27 (14)	**-2.6**	249 (260)	-17	51 (22)	0.5
	CDR EASE grid 78% SIC	48 (11)	**-3.1**	164 (118)	**-16.3**	58 (13)	-1.8
Indian	JRA-CESM 85% SIC	21 (13)	**-4.1**	167 (132)	-16.2	45 (14)	**-3.8**
	JRA-CESM 0.4m SIT	84 (31)	**-9.6**	191 (61)	5	69 (14)	-1.3
	CDR 85% SIC	54 (19)	0.1	97 (76)	1.1	45 (9)	0.8
	CDR EASE grid 78% SIC	59 (15)	0.9	114 (29)	-3.1	48 (7)	1.4
Pacific	JRA-CESM 85% SIC	0.1 (0.5)	0	72 (46)	-7.8	16 (5)	0.5
	JRA-CESM 0.4m SIT	97 (25)	-3.2	134 (58)	1.6	59 (8)	0
	CDR 85% SIC	107 (30)	5.7	58 (37)	9	58 (11)	**4.9**
	CDR EASE grid 78% SIC	87 (18)	2.9	80 (19)	0.7	57 (7)	**2.6**

Table 2. Linear trends in regional monthly polynya area. Trends are in units 10^3 km^2/decade. Products and thresholds are calculated
375 **using products on the CESM nominal 1° grid and monthly data. Bold text indicates trends that are at 95% or higher significance**

based on the Mann-Kendall non-parametric significance test (Mann 1945, Kendall 1975, Gilbert 1987). Dashed lines indicate region and season when no polynyas were identified using that product and metric at least 1/3 of the months in the timeseries.

4.3 Impacts of different definitions for sea ice concentrations in the model and satellite data

380   Discrepancies between wintertime polynya identification using SIC in the model and the satellite data may be related to differences in SIC definitions in the satellite versus model data. As discussed above, sea ice can form immediately in the model during the cold austral winter and lead to SICs that are high even though the ice may be very thin. Satellite imagery cannot differentiate between water and sea ice at very low SICs or low sea ice thicknesses. To understand potential impacts that these model and observational differences in SICs may have in polynya identification metrics, we degrade the model SIC output to

385   more closely mimic satellite estimates of SIC. In areas of low (<10% SIC) or thin (<5cm SIT) ice, we set daily SICs to 0% SIC, and in thin ice areas (5-20 cm SIT) the originally modeled SIC are reduced by half. We then identify polynyas using an 85% SIC threshold on the degraded model output.

Comparisons of the standard model to degraded output indicate that degrading SICs results in small differences that are largest

390   within the ice pack during ice growth season and along the ice edge in the winter (Appendix C and Supplemental Figs. 4-5); differences from degraded output during the sea ice retreat season (OND) are much smaller with no discernible patterns (not shown). Degrading the model data results in lower SICs throughout much of the fall pack ice and along the winter sea ice edge, and these differences show very little regional variability and do not consistently explain the model bias of the non-degraded data compared with the satellite product and in some cases would further increase model-observational biases (Supplemental

395   Figs. 4-5). Identifying polynyas based on the degraded model data (using an 85% SIC threshold) results in an increase in fall and wintertime polynyas by ~10-20% (Fig. 5 and Supplemental Fig. 6). This increase is quite small compared to the model versus CDR observation difference between polynya areas estimated using the same SIC threshold (85%). Thus, it does not explain the differences in polynya areas estimated from these two products and we focus on results using the standard model output (non-degraded) for the remainder of this paper.

Total coastal polynya area
1979-2020
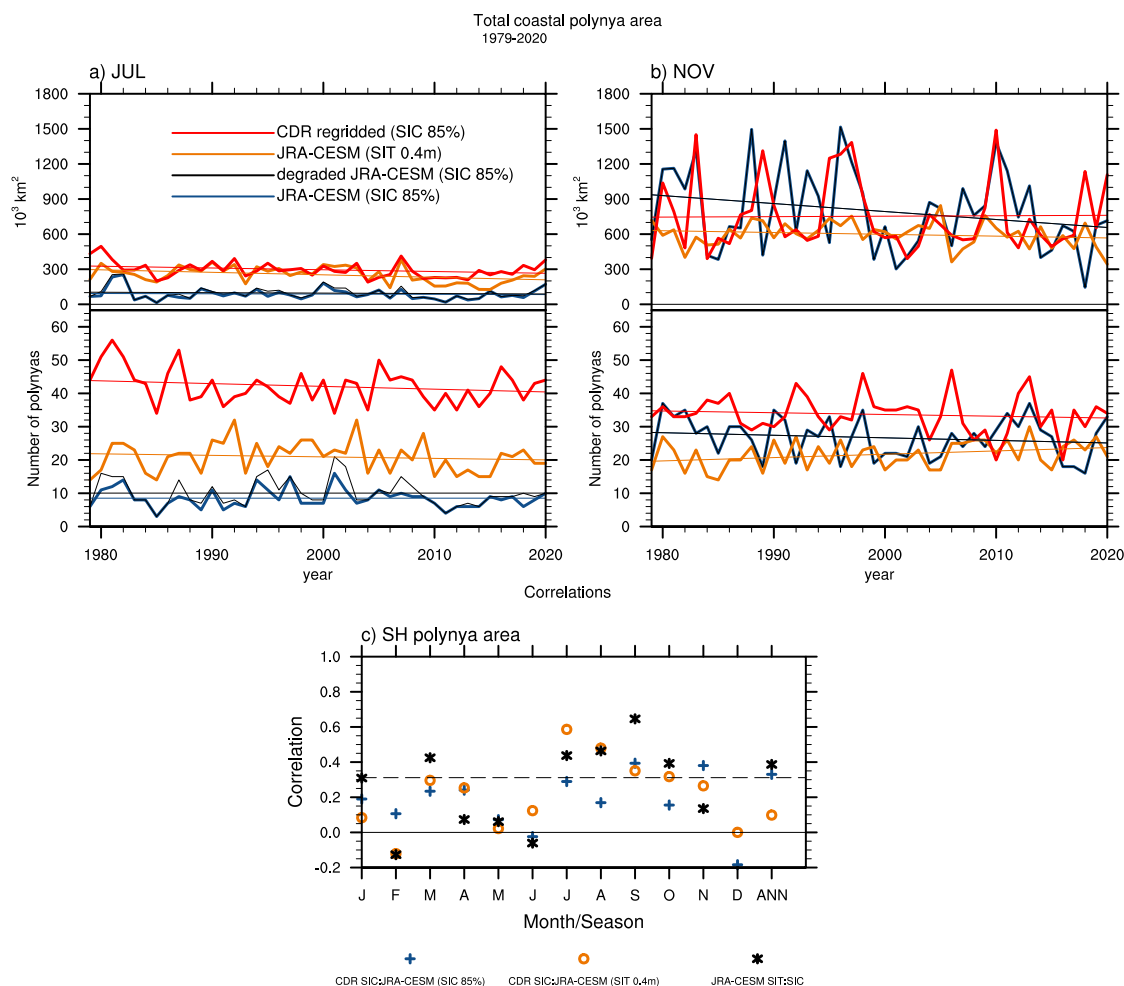
Correlations

Figure 5. Southern Hemisphere (SH) mean coastal polynya area (a-b; top panels) and number of individual polynyas (a-b; bottom panels), 1979-2020 a) July, b) November, and c) the temporal correlations between mean SH coastal polynya areas as a function of month. Polynya timeseries are for the SSMI CDR data regridded onto the CESM grid (red; 85% SIC), the JRA-CESM model simulation using monthly SIC (85%; dark teal) and SIT (0.4m; orange), and the JRA-CESM model SIC degraded to more closely mimic satellite SICs (85%; black). Thin solid lines indicate the long-term Theil-Sen non-parametric linear trends. Correlations between polynyas from the CDR (85%SIC) and JRA-CESM are shown in blue crosses/orange circles for SIC 85%/SIT 0.4m thresholds. Black * indicate correlations between polynyas identified using the monthly JRA-CESM and the two metrics (SIC 85% and SIT 0.4m).

18

4.4 Polynyas in the model hindcast simulation vs satellite observations

4.4.1 Integrated southern hemisphere polynya area

Polynya-like features have been found in CESM2 (DuVivier et al., 2021; Singh et al., 2020), and the CESM2 reproduces many characteristics of Antarctic sea ice quite well, making it a suitable model for closer investigation of polynya-like features. Polynyas identified in the model and the observations may disagree if the model doesn't adequately capture mechanisms for producing polynyas or due to model bias. It is also possible that identification of polynyas in model output may require different metric choices than those used to identify polynyas in satellite products due to differences in model vs satellite data as outlined above. We begin our comparison of polynyas in the model and the observations by calculating integrated SH total polynya areas across a range of thresholds, resolutions and seasons for both observation- and model-based data and during different seasons (Fig. 3 and Supplemental Figs. 2-3)

Polynya maps for the example day, July 15, 2003, show how the 85% SIC threshold identifies far fewer polynyas in the JRA-CESM than in the CDR (Fig. 2), suggesting that SIC may not identify polynya-like areas in model output in the winter season. Indeed, monthly climatological (1979-2020) SH polynya areas remain very small in the JRA-CESM across the full range of SIC thresholds for fall through mid-winter (April-July; Fig. 3c and Supplemental Fig. 3). During freeze up and winter, open water can re-freeze very quickly in the model, resulting in high SICs and yet relatively thin SITs. Monthly climatologies of SH polynya area reveal that SIT thresholds identify large areas of polynya throughout the fall and winter across a range of SIT thresholds, unlike SIC thresholds (Fig. 3c and Supplemental Fig. 3). Comparing polynyas identified in the satellite observations and the model output, we find that on a climatological, hemispheric basis, the best correspondence between SH polynya areas identified in the model and the observations differ by month: model simulated polynya areas identified using a 0.4 m SIT threshold correspond well to the observations in late fall through early spring (April-October), whereas SIC of 85% in the model output for late spring months (November) more closely correspond to those from the satellite product. Variability in the SH polynya area is highest in December and January (Supplemental Figs. 2-3), which is also when Antarctic sea ice is rapidly retreating (Fig. 1e). During these months, polynya areas identified in the observations at 85% SIC threshold fall in between those identified in the JRA-CESM using the SIT (0.4m) and SIC (85%). In February and March, when Antarctic sea ice reaches an annual minimum and begins to advance, very few polynyas are identified in observations or model output.

Figure 5 shows time series of SH polynya area and total number of SH polynyas for July and November and underscores many of the complications comparing polynyas estimated from satellite products to those estimated using climate model output on a seasonal basis. Temporal correlations for SH polynya area, 1979-2020, between the monthly CDR and JRA-CESM are significant for only a few months of the year – namely July-October for 0.4m SIT threshold and September, November and annually for 85% SIC (Fig. 4c). In July, the 0.4m SIT threshold results in SH polynya area that is both highly correlated and very close in mean value to that from the 85% SIC of the monthly regridded CDR, yet the number of discrete polynyas

identified in the satellite product are nearly double the number in the model output, and the average polynya size is ~ 42%
smaller in the observational product (Fig. 4 and Table 1). On the other hand, an 85% SIC threshold applied to the model data
445 in November lies closer in magnitude and temporal variability to the SH polynya area time-series from the satellite product
(utilizing an 85% SIC threshold). In general, polynyas derived from the CDR tend to be more numerous and smaller than those
derived from the model simulations for all seasons except summer (DJF; Supplemental Fig. 6). Interestingly, cross-correlations
between the two different polynya timeseries from the JRA-CESM (SIC at 85% threshold and SIT at 0.4 m threshold) vary
widely from month to month and are statistically significant and positive for about half of the months (March, July- Oct and
450 on an annual basis) while in other months the correlation is close to zero (Fig. 5c).

4.4.2 Regional polynya areas

We compare spatial polynya area climatologies by mapping polynya areas from one threshold each as a function of longitude
(Fig. 4). For CDR observations, we choose an SIC threshold of 78% on the EASE grid and 85% each for monthly and daily
regridded data. For the JRA-CESM we use thresholds of both SIC 85% and 0.4m SIT on monthly and daily JRA-CESM).
455 Figure 4 reveals that within the Bellingshausen-Amundsen sea region, modeled polynya areas are anemic compared to the
observations in winter (July) regardless of threshold metric. In contrast, in spring (November) the SIC threshold identifies
more modeled polynya areas in this region and they are closer to the polynya areas identified in the satellite observations. The
monthly 0.4 m SIT threshold identifies larger areas of polynyas in Eastern Antarctica than those identified in the satellite
product for both July and November. In general, the spatial correlations between polynya area as a function of longitude
460 identified in the satellite product and the JRA-CESM polynya area (Fig. 4c) are higher than they are for the SH timeseries (Fig.
5c). The regional variability seen in mean polynya area in the monthly regridded CDR is significantly correlated at all months
and on an annual basis with polynyas identified using SIT 0.4 m threshold in the modeled data, although the correlations are
higher using a 85% SIC threshold in November (Fig. 4c). Model polynyas identified using the 85% monthly SIC threshold are
not significantly correlated with those identified using SIC in the satellite product for May-July. Differences between mean
465 polynya areas calculated from daily and monthly JRA-CESM output tend to be smaller in the winter than in the fall, similarly
to the CDR-based polynyas. Cross correlations of polynya areas as a function of longitude estimated from daily model output
(both SIT and SIC) are not well correlated with polynya areas in the monthly CDR for summer months (Jan-Mar), when sea
ice concentrations are low, the sea ice edge is near the Antarctic continent, and variability is high.

4.4.3 Temporal polynya correlations and trends in observations and hindcast simulation

470 Monthly and annual correlations between timeseries of integrated polynya areas highlight further complexities when
comparing polynyas identified with different metrics and data products. On a hemispheric basis, significant correlations with
areas identified in the CDR (SIC 85% threshold) occur in July-October (September, November and Annual) for those identified
in the JRA-CESM using the SIT 0.4m (SIC 85%) threshold (Fig. 5c). Regionally, significant temporal correlations occur ~26%
(9%) of the time for the SIT 0.4m (SIC 85%) threshold - and the significant correlations vary in both time of year and region

475 (Fig. 6 and Supplemental Fig. 7). In general, polynyas identified using the SIT (SIC) threshold are more highly correlated with those in the CDR in July-August (October-November) in most regions except in the Bellingshausen-Amundsen Sea and Pacific Sector. The model captures much of the CDR mean, standard deviation and variability on a hemispheric basis using the appropriate metric (e.g. SIT in July and SIC in November); however the model does not tend to capture the temporal variability seen in the CDR timeseries consistently between regions even when capturing the mean (Figs. 5-6, Tables 1-2, and

480 Supplemental Fig. 7; see also discussion section below).
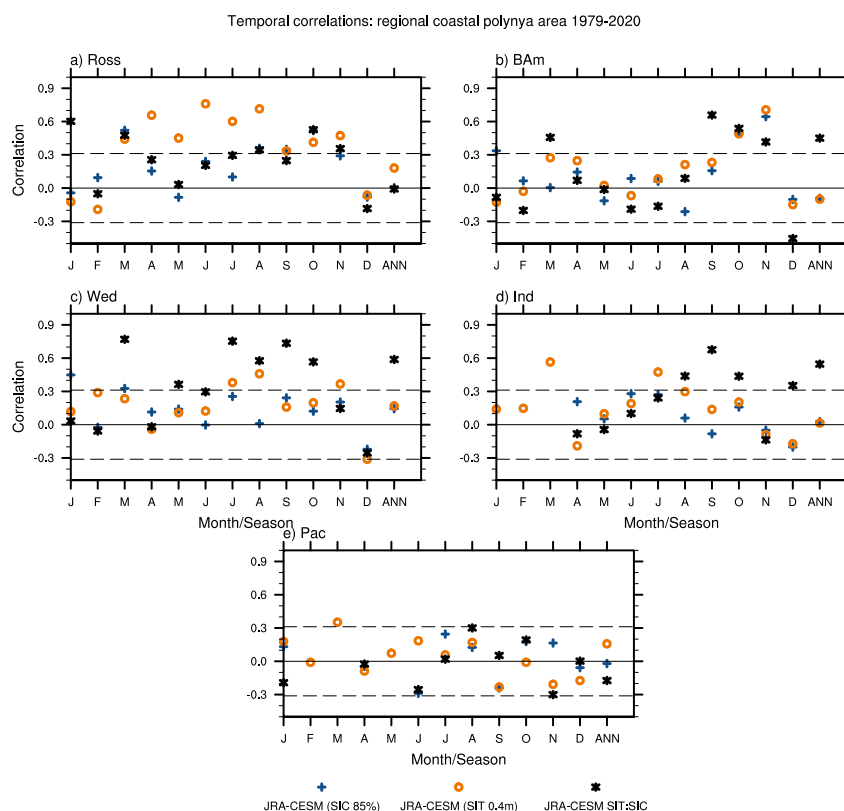
Figure 6. Regional polynya area temporal correlations for the (a) Ross, (b) Bellingshausen-Amundsen, (c) Weddell Seas and the (d) Indian and (e) Pacific sectors are calculated for timeseries identified from the monthly CDR regridded data and the monthly JRA-CESM SIT (orange circles) and the monthly JRA-CESM SIC (teal plus signs); and between the JRA-CESM SIT and JRA-CESM

485 **SIC identified polynya areas (black). The dashed lines in a-e) indicate the 95% significance levels.**

Integrated polynya areas in the JRA-CESM from both SIC and SIT thresholds are significantly correlated with each other ~34% of the months/annual basis over the five regions, most consistently in the months or September and October with the exception of the Pacific sector where they are not significantly correlated (Figs. 5, 6). By November, when simulated Antarctic

490 sea ice begins its spring retreat (e.g. Fig. 1e) and is losing volume more rapidly than extent (SH sea ice loses 22%/18% of its

annual extent loss and 33%/30% of its annual volume loss in November for the JRA/CESM2; not shown), correlations between polynyas using SIT and SIC thresholds become either less highly correlated (Ross, Bellingshausen-Amundsen Seas) or are not significantly correlated (Fig. 5-6). The generally insignificant winter (June-August) correlations between coastal polynya areas identified using in the JRA-CESM using the SIT and SIC may be at least partially due to the very low winter polynya areas

495   identified by SICs, when winter temperatures lead to rapidly forming sea ice and high SICs even in very low SIT regions. The exception is the Weddell Sea - where winter polynyas identified using both metrics are similar in mean and variability (Fig. 7 and Supplemental Fig. 7).
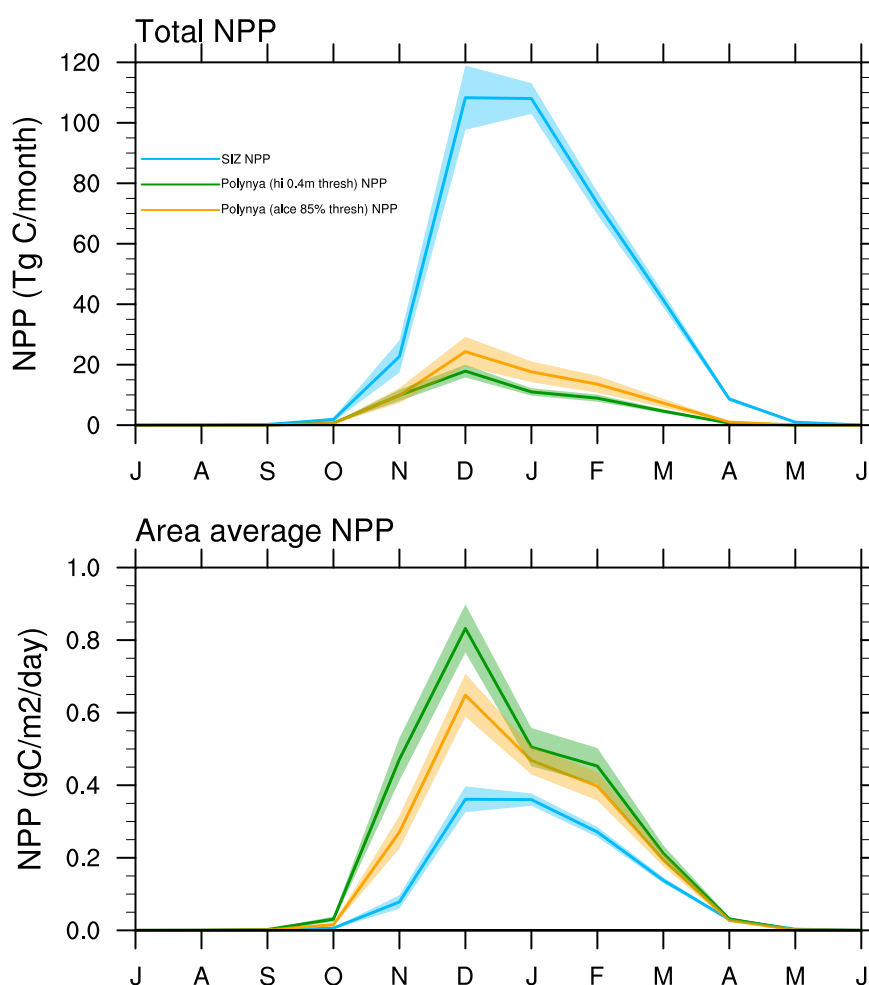
Figure 7. 1979-2020 climatological integrated SH monthly total NPP (top) and area-averaged NPP (bottom) for the sea ice zone (SIZ:
500   **blue) and SON polynya regions identified using 0.4 SIT (green) and 85% SIC (orange) thresholds.**

SH polynya areas show significant negative trends in July in the CDR (in both original-EASE and 1° grids) and the JRA-CESM using the SIT (0.4m) threshold (Table 1). On the other hand, SH trends in November and on an annual basis are

significant only in the model (November, both metrics) or in the CDR on the EASE grid (annually). Regional trends are varied
505   in sign, magnitude and season across all data sources (Table 2). Regional trends - like the integrated SH trends - are
insignificant in November except for polynyas identified in the CDR on the equal area grid for the Ross and Weddell Seas,
where they are negative (Table 2). Polynya area trends are significant and negative in July in the Ross-Bellingshausen and
Weddell Seas in one or both grids, but only in the CESM in the Indian sector. One possible source of these differences may
lie in the reanalysis product used to force the CESM-JRA, discussed in section 5.

4.5 Relationships between polynyas and NPP in the JRA-CESM

Net primary productivity (NPP) describes the rate of photosynthetically fixed carbon in the upper ocean; it quantifies the
energy available for marine food webs. In the high-latitude Southern Ocean, NPP increases markedly as the sea ice retreats
and light returns to Antarctic waters (e.g. Richert et al., 2019 and references therein). Light reaches the surface sooner in
polynyas than the surrounding ice-covered areas, relieving phytoplankton of light limitation (e.g. Arrigo & van Dijken, 2003).
515   We look at polynya regions defined in the austral spring (September, October, November, "SON"), to see if the model captures
high NPPs within identified polynyas during the early growth season. There is not a clear choice of metric - a sea ice
concentration or thickness threshold - to define the SON polynya areas based on the previous analysis that indicates that
polynyas identified using a 0.4 m SIT/0.85% SIC threshold show higher spatial and temporal correlations with those satellite
identified polynyas in September/November. We therefore use austral spring polynya regions as identified by both the 0.4 SIT
520   and the 85% SIC metrics for the NPP analysis.

Comparing the monthly average NPP per unit area within austral springtime coastal polynyas and within the sea ice zone
allows us to better understand how polynyas may augment austral spring NPP and thus play a critical role in the Antarctic food
web. Note that the SIZ, which is defined as the area covered seasonally with sea ice (as determined by the mean winter - JJA
525   - 85% SIC contour) covers significantly more ocean area than the spatial area of polynyas, so the overall production within the
SIZ is larger than in polynyas (Fig. 7a). However, we find that the NPP per unit area is substantially higher during the austral
spring in regions identified as polynyas using both SIC and SIT polynya identification methods than it is within the SIZ
generally (Fig. 7b). This finding suggests that the model does indeed capture high productivity within low and thinner ice
regions. Additionally, the higher NPP per unit area persists into the summer months as well. Polynyas have an especially large
530   impact on NPP during December, when area average NPP within polynyas is more than twice as much as within the SIZ when
using the 0.4m SIT threshold and 1.5 higher when using the 85% SIC threshold. Although the total SON polynya area is an
order of magnitude smaller than the total SIZ area, NPP within polynyas contributes ~17-23% of the total NPP during the
December peak. These results highlight the importance of polynyas to Antarctic productivity, as represented in the CESM.

4.6 CESM2-LE: Antarctic coastal polynyas and NPP in a changing climate

535 The above analysis indicates that the CESM2 is simulating polynya-like features with elevated NPP compared to the SIZ generally. Thus, we extend our analysis to the 50 member CESM2 Large Ensemble (CESM2-LE) over the historical (1850-2014) and future moderately-high emission (SSP370) scenario (2015-2100) to explore how polynyas and NPP may change in a changing climate. SH coastal polynya areas identified in the CESM2-LE using both the SIT 0.4m and SIC 85% thresholds indicate that polynya areas tend to be higher in the fully coupled CESM2-LE using the wintertime SIT threshold, as was found

540 in the JRA-CESM simulations (Fig. 8). In general, SH coastal polynya areas are smaller in the CESM2-LE particularly in November than in the JRA-CESM simulation and in satellite observations. The number of discrete wintertime coastal polynyas identified in the CDR observational products is significantly larger than from either metric in either the JRA-CESM or the fully coupled simulations (Fig. 8a). SH CESM2-LE July polynya areas identified using the SIT threshold show small increases from 1850-2100 (Fig. 8a). November SH polynya area decreases in both the SIT- and particularly in the SIC-identified areas

545 over the last 40-50 years of the 21st C (Fig. 8b).
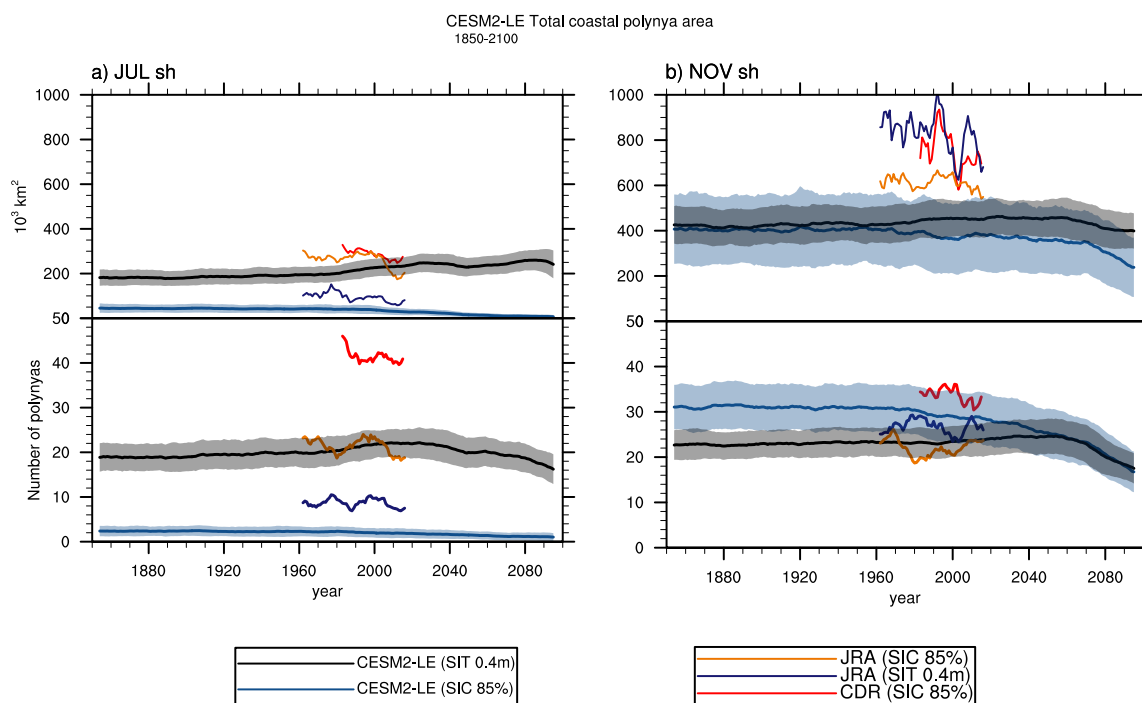
Figure 8. Integrated southern hemisphere mean coastal polynya area and number of polynyas,1979-2020, for July (left) and November (right). Polynya timeseries are created from monthly data on the nominal 1° CESM grid and shown for SSMI CDR (red; 85% SIC), the JRA-CESM SIC (85%; dark teal), the JRA-CESM SIT (0.4m; orange), and the CESM2-LE SIC (85% SIC; black)

550 **and SIT (0.4m SIT, blue). The ensemble mean for the CESM2-LE is shown by the thick line with shading indicating ±1 standard deviation.**

Trends in springtime (SON) polynya areas show broad similarities to those in July and November, with polynya areas identified using the SIC metric declining starting in the latter half of the 20th century, and increasing until about 2050 in the SIT threshold

555 and then decreasing (Fig. 9d). The differences in trends between polynyas identified using SIT and SIC thresholds may be related to the more rapid decline in sea ice volume compared with sea ice extent in austral spring during the latter half of the 21st century (not shown). SIT associated polynya areas are about 50% higher than the SIC-polynya areas until that latter part of the 20th C, when SIC-associated polynya areas decrease through the remainder of the simulations. SON polynya areas identified using the SIT metric increase from the latter part of the 20th century until the latter half of the 21st century, when

560 they begin to decrease. A more detailed seasonal and regional analysis of these trends along with an exploration of the differences between SIT and SIC metric is beyond the scope of this work.
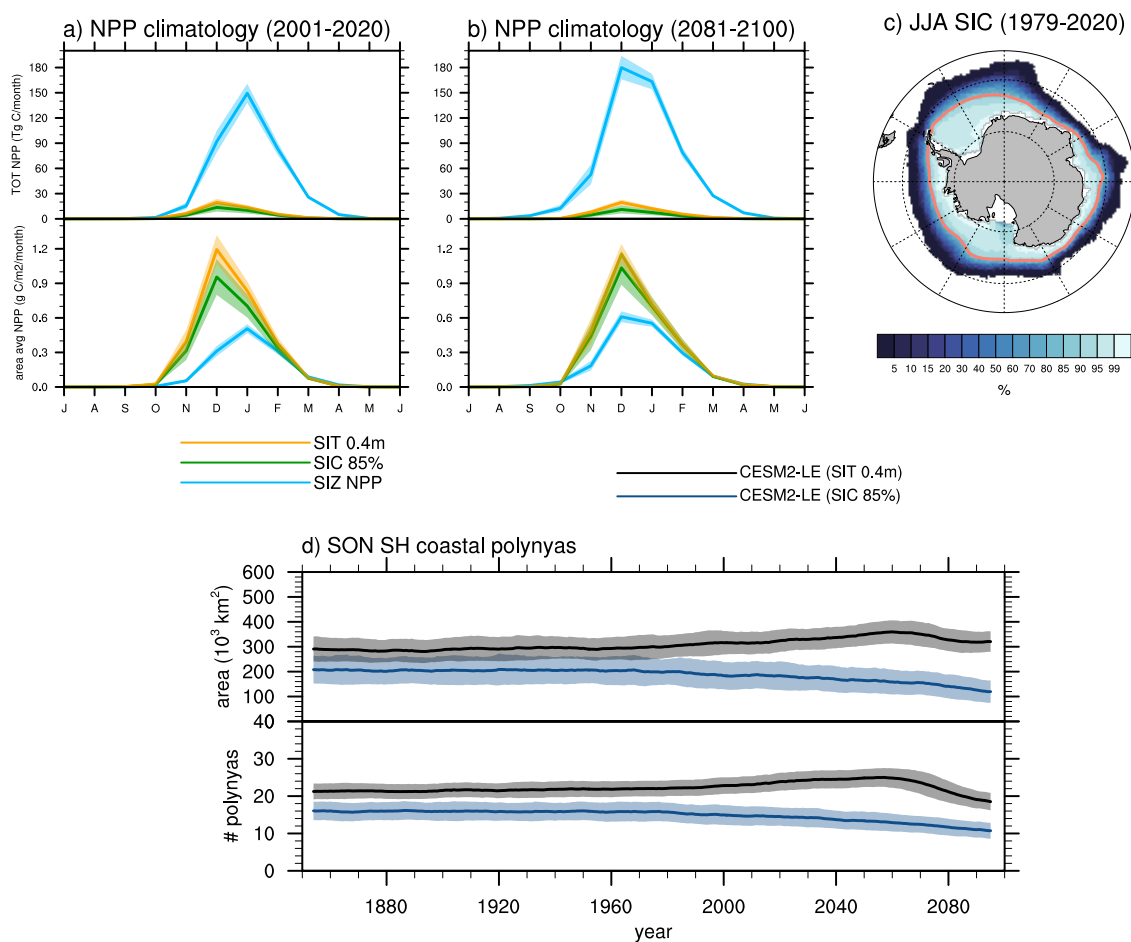
Figure 9. Monthly climatology for total (top) and area average (bottom) NPP for a) first (2001-2020) and b) last (2081-2100) 20 yrs of the 21st Century; c) climatological 1979-2020 winter (JJA) SIC with sea ice zone (SIZ; 85% SIC contour shown in red); and

565 **integrated SH spring (SON) d) polynya area (top) and number of polynyas (bottom). NPP is shown within the SIZ (light blue), the SIT-0.4 m polynyas (orange) and the SIC-85% polynyas (green). Solid lines/shading in a-b indicate ensemble mean/±1 standard**

deviation. SON SH coastal polynya areas and numbers are shown as a 10 yr running ensemble mean (solid line) and ±1 standard deviation (shading).

570 As in the JRA-CESM simulation, area average NPP in the CESM2-LE is much higher within polynyas than within the SIZ on a per area basis (Fig. 9a-b). SIZ-NPP in the CESM2-LE peaks in January in 2001-2020, later than the December peak NPP observed in the JRA-CESM. Ensemble mean SIZ-NPP increases markedly in the 21st century under the moderately high emission scenario, particularly in the early growth season (December) and such that there is a distinct December peak in the climatological SIZ-NPP by 2081-2100. In addition to the changing seasonality of NPP in the SIZ, area average SIZ-NPP and

575 total SIZ-NPP increase in the future scenario. Although polynya areas identified using the SIT are higher than those identified using the SIC metric (Fig. 9d), area average NPP becomes higher at the end of the century within the low SIC polynyas during the peak of the spring bloom, with the result that total integrated SIZ NPP is slightly larger (Fig.9a-b). Area average NPP within the polynya areas shows much smaller changes than within the SIZ, with slight increases/decreases within SIT/SIC identified polynyas during the December peak. NPP within polynyas contributes a small portion of the total NPP by the end

580 of the 21st Century (Fig. 9b). Changes in seasonality of the SIZ NPP may be accompanied by changes in efficiency of trophic transfer (i.e. the dominant phytoplankton types may shift, as shown in Krumhardt et al. 2022) – analysis of trophic level changes in a changing climate are left for future analysis.

5 Discussion

Polynyas are often subjectively defined -- "open water surrounded by ice and/or ice and land" -- and a leading conclusion of

585 this work is that care must be taken when identifying polynyas quantitatively from gridded data. This is particularly important for comparisons between products with different definitions of SICs (e.g. remotely sensed snapshots of observed sea ice conditions vs modeled sea ice concentrations from thermodynamic and dynamic numerical equations). Ideal metrics and metric thresholds for polynya identification will depend on the product grid sizes, region of interest, season and application, as well as the specifications of an individual data product. Even satellite-based SICs on the same grid can differ based on SIC retrieval

590 algorithms, as demonstrated here by the typically higher number and area of polynyas identified by the NASA Team algorithm than by the CDR for the same SIC threshold. Additionally, satellite-based SICs from the same product on different grids can also lead to different results when identifying polynyas. Nonetheless, below we provide some "best practices" from this systematic comparison of polynya identification methods and discuss the implications of polynya metric choices for applications in climate models.

595 **5.1 Polynya metric choices: Temporal and spatial resolutions**

Analysis of polynyas identified in both satellite and model products suggest that annual climatologies made from daily vs monthly data do not differ significantly, and thus monthly data may be sufficient for many analyses both from observations

and climate model output on larger scales. In general, polynya areas defined by the same SIC threshold and product will be slightly larger using daily data than monthly data. There are seasons and regions, however, that show significant differences

600 in polynya areas between daily data and monthly data at the same threshold value, and when monthly data may lead to larger polynya area identification – e.g. in the Ross and Weddell Seas from late spring through late summer (November-March).

Grid resolution significantly impacts polynya metric and threshold choices and a given threshold value will lead to significantly larger polynya areas on a higher resolution grid than on a lower resolution grid. A constant SIC metric results in different areas

605 of polynyas when used on an equal area grid than on a equal-degree grid (e.g. Appendix), which may explain our differing results in trends seen from polynya areas identified in the CDR on the EASE vs 1° grid. In order to eliminate discrepancies due to grid types and resolutions alone, we recommend comparing metrics from data on the same grid, and regridding - if necessary - data with the higher geographical resolution onto the lower resolution grid.

5.2 Polynya product and metric choice in modeled data

610 Using SICs, in general, to identify SH wintertime coastal polynyas in model simulations requires very high thresholds and is particularly problematic in the Bellingshausen-Amundsen Sea. Part of this issue is likely because ocean surface waters can very rapidly refreeze and form very high sea ice concentrations in all models, not just the CESM. Degrading model output to more closely resemble satellite estimates of SICs leads to only small increases in polynya areas identified using SICs (at 85% threshold) and does not explain the large bias between polynyas identified in July by the CDR and JRA-CESM using 85% SIC

615 thresholds. A more direct comparison between SICs as a metric to identify polynyas in both simulated and observed data could be made with the use of a satellite-simulator in the model to calculate brightness temperatures as a satellite would measure them (e.g. Smith et al., 2021). Wintertime polynya-like features are identified in the CESM using daily SICs along the eastern Antarctic coast, and yet not in the Bellingshausen Sea (e.g. Fig. 4) suggesting that there may be model biases in the CESM impacting regional sea ice dynamics.

620

While SIT is not available in long term satellite observations as an identification metric, SITs readily identify wintertime polynya areas in models across a range of thresholds and for all regions. In addition, variability is more strongly correlated for CDR and JRA-CESM wintertime polynyas identified using 85% SIC from observations and 0.4m SIT from the model. SITs continue to successfully identify modeled polynyas as the ice begins its retreat in September-October, although by November,

625 SICs identify polynya areas in the model output across a range of thresholds and of similar magnitudes as found in the regridded CDR data. This study assesses only the CESM2 model, and more work should be done to test if the seasonality of SIC and SIT as a polynya identification threshold differs by model. Polynyas identified in the model output are significantly correlated geographically for both SIC and SIT thresholds with those estimated from the CDR data in November. We thus find that identification of wintertime polynyas in the CESM better reproduces observed polynyas when using a SIT-based threshold,

630 which more accurately accounts for low sea ice areas than SICs, which can be very high in the model even in   very thin sea

ice conditions, unlike in satellite imagery. We suggest using a SIT-based metric for winter-time polynya identifications in model output. SITs continue to serve as a good metric for polynya identification in model output in the early spring when sea ice is still quite extensive, although SIC metrics tend to perform better as the sea ice thins and sea ice extent begins a rapid retreat - which is in November in the CESM but may differ somewhat in timing in other models (e.g. Roach et al., 2020). We

635   recommend considering both SIC and SIT based metrics for polynya identification in the austral spring.

It is interesting to note that while significant longitudinal correlations exist between polynya areas identified in the CESM-JRA and the CDR for each month of the year and annually (Fig. 4c), the same cannot be said for temporal correlations of the integrated time series (Figs. 5c and 6a-e). This suggests that the regionality of the identified polynyas in the CESM-JRA is

640   captured well compared to the observations, however the temporal variability is less well captured in some regions and seasons. Part of this may be explained by the reanalysis data used to force the CESM-JRA and the nature of coastal polynyas. Reanalysis wind products show the lowest biases compared with weather station data in regions and times of high synoptic and/or low katabatic wind activity, and significant biases in wind fields close to the coast near where katabatic winds significantly impact coastal winds (e.g. Jones et al., 2016; Harrison et al., 2022). Katabatic winds are integral to the formation of coastal polynyas

645   (e.g. Thompson et al., 2020 and references therein). Thus, coastal polynya variability due to variability in katabatic winds may be captured by the polynya time series in the observations but not well represented in the atmospheric reanalysis data used to force the model.

Recent work found significant positive trends in annual polynya areas in the Ross, Weddell, Indian and Pacific sectors

650   estimated using daily data from the EUMETSAT data product at a 50% threshold on a 25 km x 25 km equal-area grid (Duffy et al., 2023). Our results show significant positive trends only in the Pacific sector, and significant negative trends in both the Bellingshausen-Amundsen and Ross Sea in polynya areas identified in the CDR on the EASE grid. This contradiction must be due to differences in satellite data products, metrics or methods used to identify polynyas - an analysis beyond the scope of this work - yet it highlights that caution should be taken when comparing results from different sources, grids, methods and

655   metrics.

5.3 Polynya applications: polynyas and NPP in a changing climate

Our analysis with the CESM2-LE demonstrates using a 0.4 m SIT and an 85% SIC metric to identify polynyas in the austral spring (SON) result in larger ensemble mean areas of polynyas in the SIT-identified polynyas than in the SIC-identified ones. Contributions to NPP are quite similar in both SIC and SIT-defined polynyas, and polynyas identified using both metrics show

660   substantial augmentation of Antarctic NPP within polynyas compared to within the entire SIZ, indicating that the CESM is indeed capturing enhanced productivity within polynya-like features in austral spring. Changes in NPP within polynyas are small compared to those within the SIZ, which increases substantially and changes seasonality by the end of the 21st Century. This analysis demonstrates that the CESM may be a useful tool to investigate changing Antarctic marine ecosystems within

polynyas and the sea ice zone in a warming climate. As the climate warms and sea ice responds, better understanding how to

665 identify polynyas in different regions or seasons will be critical for quantifying how production in the ocean around Antarctica

may change including timing of peak NPP production, changes in trophic transfer and species composition, etc.

6 Conclusions

The definition of "polynyas" in a quantifiable sense is relatively subjective. Defining areas and timing of open water within

the Antarctic sea ice zone such that comparisons can be made between satellite based SICs and model output require careful

670 consideration and recognition of the basic differences between satellite observations and model output. It is critical to consider

grid type and resolution, season, metric and threshold as optimal metrics chosen may depend on region and season of interest.

Our six primary recommendations are:

1) all data should be regridded to the same type and size of grid for comparisons to reduce differences due to grids
675   alone
2) polynya areas identified from monthly and daily data are comparable on hemispheric basis
3) sea ice thicknesses are a more suitable metric for identifying polynyas in climate model data in the winter months
4) sea ice concentrations are a more suitable metric for identifying polynyas in the late spring in climate model data, when sea ice is rapidly retreating, though this may be model dependent
680 5) optimal metric and threshold choices will be influenced by grids, regions, and seasons of interest
6) productivity within polynya areas may help evaluate model performance with respect to capturing enhanced productivity in polynya-like features, as seen in observations.

Appendice

Appendix A: Polynya algorithm

685 The polynya algorithm cycles through maps of the sea ice variable (concentration or thickness in this work) and initially labels

any grid cells that fall below the threshold and that lie within the sea ice zone (south of the open ocean boundary). The algorithm

iteratively cycles through the polynya maps to determine if grid cells that meet the threshold criteria are surrounded by sea ice

and land (in which case they are labeled a polynya) or lie next to open ocean (in which case they are not identified as a polynya).

Figure AA1 shows a schematic of a hypothetical region with land, ocean, sea ice and polynya grid cells. In this example, there

690 are two polynyas – one open water polynya (occupied by three grid cells), and one coastal polynya (occupied by two grid

cells). Figure AA2 shows an example satellite image of the Ross Bay and Terra Nova polynyas and grid cells labeled by SICs.

No = not polynya

OWP = open water polynya

CP = coastal polynya

695

	0% SIC (open ocean)
	< threshold (e.g. 50% SIC)
	> threshold (e.g. 90% SIC)
	Land

Figure A1. Schematic of grid cells considered open ocean (dark blue), land (light green) and within the sea ice zone (light and medium blue). Grid cells in the sea ice zone that meet the threshold criteria are in medium blue; grid cells that lie above the threshold are in light blue. Grid cells that meet the criteria are identified as polynyas only if they are bounded by sea ice (open water polynyas) or
700 **sea ice and land (coastal polynyas).**
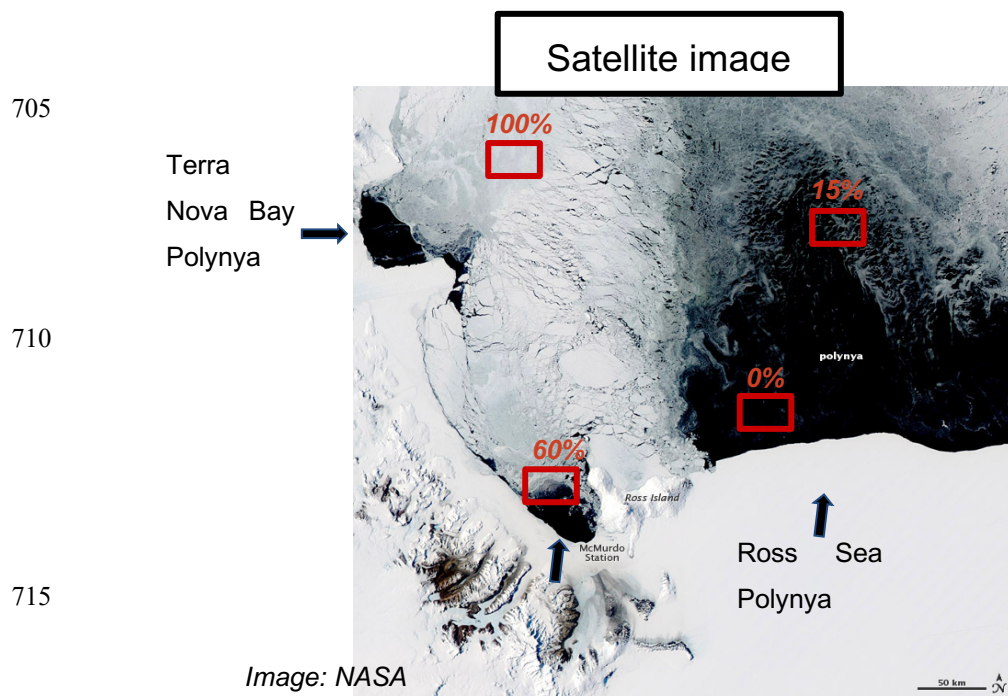
Figure A2. Example satellite image of the Terra Nova Bay and Ross Sea polynyas (REF). Hypothetical grid cells with SICs are shown in red.

Appendix B: Grid size and type and impact on polynya definitions

Using concentration thresholds to define polynya regions will define how much open water (or sea ice) is in the grid cell by percentage. For an Equal Area Scaleable Earth (EASE) grid this will correspond to an area that doesn't change with latitude or longitude, whereas on an equal latitude-longituide grid a SIC percent threshold will correspond to different areas of open water (or sea ice) depending on latitude. For example, a 50% sea ice concentration threshold on a 25kmx25km EASE grid corresponds to 312.5 km^2 or more of open water (and also 312.5 km^2 of sea ice) within the grid cell to meet the threshold requirement for a polynya. A grid based on latitude and longitude, which is common for earth system models, will have a varying range of surface area in each grid cell. Figure AB1 shows the sea ice concentration at which a grid cell on the CESM grid (~1°x1° lat/long) will contain 312.5 km^2 of open water, or the same area of open water as on a grid cell on an EASE grid that has 50% SIC. An example of the SIC thresholds required to result in 312.5 km^2 of open water within a grid are shown in Fig. AB2 for an equal area grid cell and two grid cells from a 1°x1° grid cell at two different latitudes. Different grid sizes can also lead to different numbers of polynyas even when the areas are the same (e.g. Fig. AB3).

31

SIC threshold (CESM grid) for
50% SIC threshold on 25 km² grid
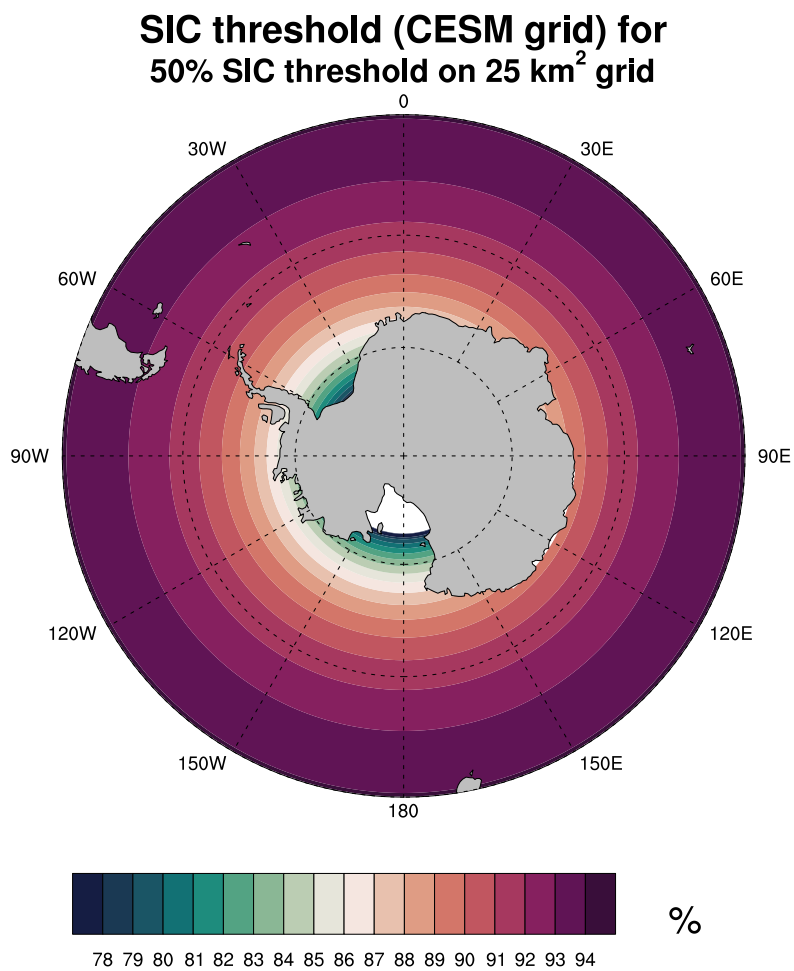
735   **Figure B1. Sea Ice Concentration required to result in 312.5 km² open water within a grid cell on the CESM nominal 1° grid.**
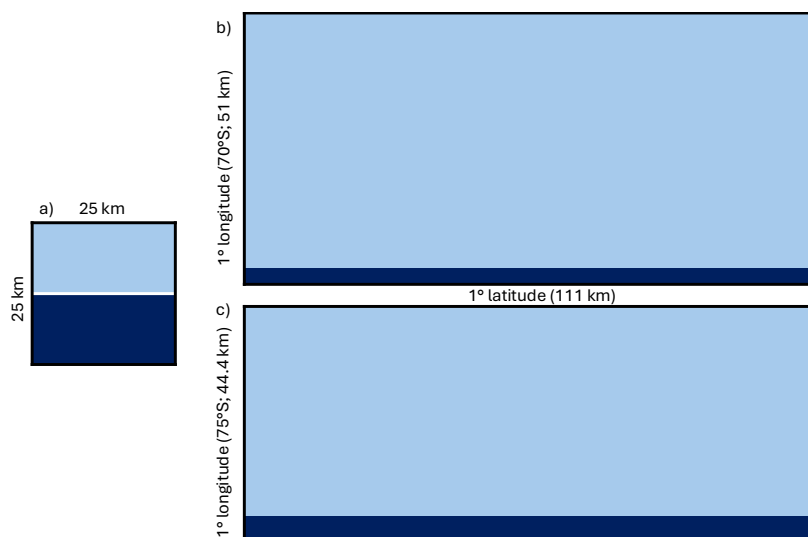
740

Figure B2. Sea ice concentration required to result in 312.5 km² of open water within a grid cell: a) SIC 50% on a 25km x 25k equal area grid cell, b) 92% SIC on a 1°x1° lat/lon grid cell at 70°S (approximately 111km x 51km), and c) 84.4% SIC on a 1°x1° lat/lon grid cell at 75°S (approximately 111km x 44.4km)
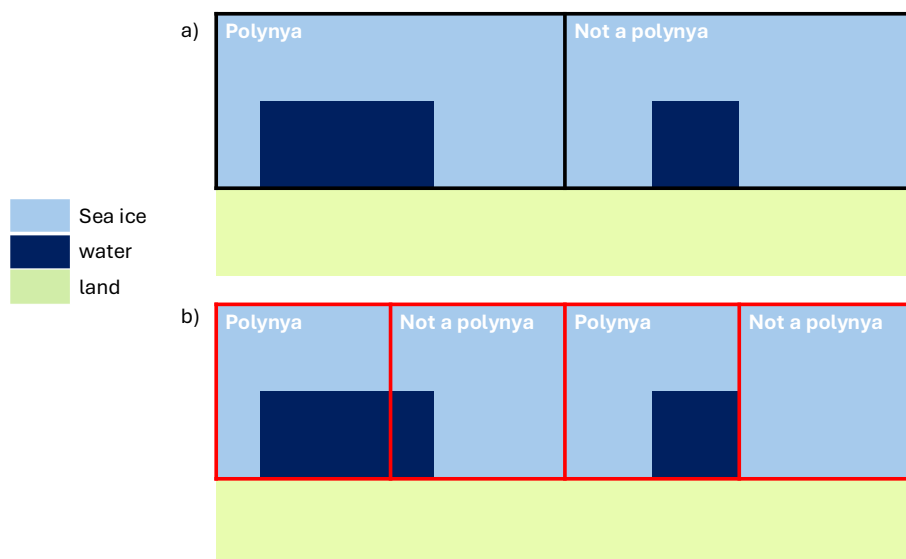
745

Figure B3. Examples of grid cells classified as polynyas using a 75% SIC threshold on a larger resolution grid (a) and a smaller resolution grid (b). Both figures have the same total integrated polynya area over the region, however there is only one polynya grid cell in (a) and two polynyas in (b).

750 **Appendix C: Degrading climate model daily SIC data.**

Figure AC1 shows an example of model SICs that are degraded such that the new sea ice concentrations are set to 0 where the original SICs are less than 10% and also where SITs are less than 5 cm. In regions of SITs that fall between 5cm and 20 cm, SICs are set to half of the original values. The resulting degraded product has noticeably lower SICs along the ice perimeter and isolated locations near the Antarctic continent with lower SICs.

755
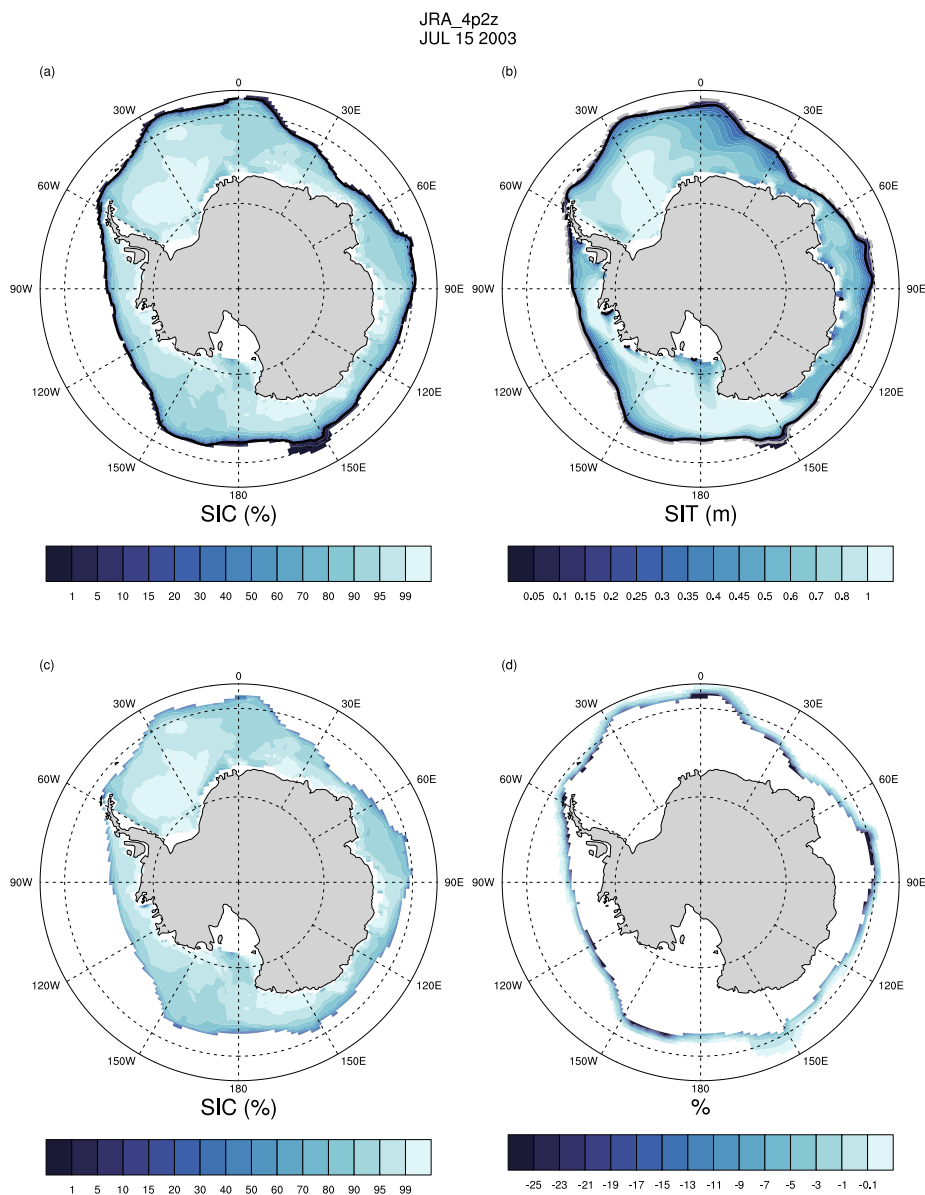
Figure C1. Sea Ice Concentration (a) and sea ice thickness (b) from the JRA-CESM run on July 15, 2003. Degraded sea ice (c) and the resulting change in SIC by degrading the sea ice.

Code and data availability

The CESM2-LE data used in this study are freely available, as described in Rodgers et al. (2021). The CESM2-LE and the JRA hindcast simulations (Forced Ocean Sea Ice, FOSI) are freely available from the Earth System Grid

765 (https://www.earthsystemgrid.org/project/CESM.html). The computational notebooks and other data processing tools used for this publication are freely available online (L.Landrum, 2024). Code for processing the data and making the figures will be published on a GitHub repository in final stages if paper is accepted for publication.

Author contributions

Study design and analysis were conducted by LL with ideas from MMH, AKD, KK and ZS. All authors contributed to the writing of the manuscript.

770 **Competing Interests**

The authors declare that they have no conflict of interest.

References

Arrigo, K. R., and G. L. van Dijken, G. L.: Phytoplankton dynamics within 37 Antarctic coastal polynyas, J. Geophys. Res., 108(C8), 3271, doi:10.1029/2002JC001739, 2003.

Comiso, J. C., Cavalieri, D., Parkinson C., and & Gloersen, P.: Passive microwave algorithms for sea ice concentrations: a 790 comparison of two techniques. Remote Sensing of the Environment, 60, 357 384, 1997.

Danabasoglu, G., Lamarque, J. F., Bacmeister, J., Bailey, D. A., DuVivier, A. K., Edwards, J., et al.: The Community Earth System Model version 2 (CESM2). J. Adv. in Model. Earth Sys., 2, 1–35. https://doi.org/10.1029/2019ms001916, 2020.

Duffy, G. A., Montiel, F., A. Purich, A. and C. I. Fraser, C. I.: Emerging long-term trends and interdecadal cycles in Antarctic polynyas, Proc. of the Nat. Acad. of Sc., 121 (11), https://doi.org/10.1073/pnas.2321595121, 2024.

795 DuVivier, A. K., Holland, M. M., Landrum, L., Singh, H. A., Bailey, D. A., and Maroon, E. A.: Impacts of sea ice mushy thermodynamics in the Antarctic on the coupled Earth system, Geophys. Res. Lett., 48, e2021GL094287, https://doi.org/10.1029/2021GL094287, 2021.

Eyring, V., Bony, S., Meehl, G. A., Senior, C. A., Stevens, B., Stouffer, R. J., and Taylor, K. E.: Overview of the Coupled Model Intercomparison Project Phase 6 (CMIP6) experimental design and organization. Geosc. Model Devel., 9(5), 1937–
800 1958, https://doi.org/10.5194/gmd-9-1937-2016, 2016.

Fetterer, F., Knowles, K., Meier, W. N., Savoie, M. and Windnagel, A. K.: Sea Ice Index, Version 3. Distributed by National Snow and Ice Data Center, Boulder, Colorado, USA (accessed 2 June 2023); https://doi.org/10.7265/N5K072F8, 2017.

Flores, H., Veyssière, G., Castellani, G. *et al.*: Sea-ice decline could keep zooplankton deeper for longer. Nat. Clim. Chang. 13, 1122–1130, https://doi.org/10.1038/s41558-023-01779-1, 2023.

805 Fogt, R. L., Sleinkofer, A. M., Raphael, M. N. *et al.:* A regime shift in seasonal total Antarctic sea ice extent in the twentieth century. Nat. Clim. Chang. 12, 54–62, https://doi.org/10.1038/s41558-021-01254-9, 2022.

Gilbert, R. O.: Statistical Methods for Environmental Pollution Monitoring, Wiley, NY, 1987.

Harrison, T. C., Biri, S., Bracegirdle, T. J., King, J. C., Kent, E. C., Vignon, É., and Turner, J.: Reanalysis representation of low-level winds in the Antarctic near-coastal region, Weather Clim. Dynam., 3, 1415–1437, https://doi.org/10.5194/wcd-3-
810 1415-2022, 2022.

Ivanova, N., Pedersen, L. T., Tonboe, R. T., Kern, S., Heygster, G., Lavergne, T., Sorensen, A., Saldo, R., Dybjkaer, G., Brucker, L. and Shokr, M.: Inter-comparison and evaluation of sea ice algorithms: towards further identification of challenges and optimal approach using passive microwave observations, The Cryo., 9, 1797-1817, https://doi.org/10.5194/tc-9-1797-2015, 2015.

815 Jones, R., Renfrew, I., Orr, A., Webber, B., Holland, D., and Lazzara, M.: Evaluation of four global reanalysis products using in situ observations in the Amundsen Sea Embayment, Antarctica, J. Geophys. Res.-Atmos., 121, 6240–6257, 2016.

Kacimi, S., and Kwok, R.: Arctic snow depth, ice thickness, and volume from ICESat-2 and CryoSat-2: 2018–2021. Geophys. Res. Letts., 49, e2021GL097448. https://doi.org/10.1029/2021GL097448, 2022.

Kendall, M.G.: Rank Correlation Methods, 4th edition, Charles Griffin, London, 1975.

820 Kern, S., Spreen, G., Kaleschke, L., De La Rosa, S., and Heygster, G.: Polynya Signature Simulation Method polynya area in comparison to AMSR-E 89GHz sea-ice concentrations in the Ross Sea and off the Adélie Coast, Antarctica, for 2002–05: first results, Ann. Glaciol., 46, 409–418, 2007.

Kobayashi ,S., Yukinari, O. T. A., Harada, Y., Ebita, A., Moriya, M., Onoda, H., Onogi, K, Kamahori, H., Kobayashi, C., Miyaoka, K., Takahahi, K.: The JRA-55 reanalysis: general specifications and basic characteristics. J Meteorol Soc Jpn Ser II
825   93(1), 5–48, https://doi.org/10.2151/jmsj.2015-001, 2015.

Krumhardt K. M., Long, M. C., Sylvester, Z. T. and Petrik, C. M.: Climate drivers of Southern Ocean phytoplankton community composition and potential impacts on higher trophic levels. Front. Mar. Sci. 9:916140. doi: 10.3389/fmars.2022.916140, 2022.

Krumhardt, K. M., Long, M. C., Petrik, C. M., Levy, M., Castruccio, F. S., Lindsay, K., Romashkov, L., Deppenmeier, A.-L.,
830   Denéchère, R., Chen, Z., Landrum, L., Danabasoglu, G. and Chang, P.: From nutrients to fish: Impacts of mesoscale processes in a global CESM-FEISTY eddying ocean model framework, Prog. in Ocean., 227, 2024, 103314, ISSN 0079-6611, https://doi.org/10.1016/j.pocean.2024.103314, 2024.

Labrousse, S., Fraser, A. D., Sumner, M., Tamura, T., Pinaud, D., Wienecke, B., et al.: Dynamic fine-scale sea icescape shapes adult emperor penguin foraging habitat in East Antarctica. Geophys. Res. Lett. 46, 11206–11218. doi:
835   10.1029/2019GL084347, 2019.

Lavergne, T., Sørensen, A. M., Kern, S., Tonboe, R., Notz, D., Aaboe, S., Bell, L., Dybkjær, G., Eastwood, S., Gabarro, C., Heygster, G., Killie, M. A., Brandt Kreiner, M., Lavelle, J., Saldo, R., Sandven, S., and Pedersen, L. T.: Version 2 of the EUMETSAT OSI SAF and ESA CCI sea-ice concentration climate data records, The Cryo., 13, 49–78, https://doi.org/10.5194/tc-13-49-2019, 2019.

840   Li, Y., Ji, R., Jenouvrier, S., Jin, M. and Stroeve, J.: Synchronicity between ice retreat and phytoplankton bloom in circum-Antarctic polynyas, Geophys. Res. Lett., 43, 2086–2093, doi:10.1002/2016GL067937, 2016.

Mann, H.B.:Non-parametric tests against trend, Econometrica 13:163-171, 2045.

Markus, T. and Burns, B. A.: Detection of coastal polynyas with passive microwave data. Ann. Glaciol. , 17, 351- 355, 1993.

Massom, R. A., Harris, P. T., Michael, K. J., and M. J. Potter, M. J.: The distribution and formative processes of latent-heat
845   polynyas in East Antarctica, Ann. Glaciol., 27, 420– 426, 1998.

Meier, W.N.: Comparison of passive microwave ice concentration algorithm retrievals with AVHRR imagery in Arctic peripheral seas. IEEE Trans. Geo. Remote Sensing, 43, 1324-1337, 2005.

Meier, W. N., Peng, G., Scott, D. J., and Savoie, M. H.:. Verification of a new NOAA/NSIDC passive microwave sea-ice concentration climate record. Polar Research, 33. doi: 10.3402/polar.v33.21004, 2014.

850   Meier, W. N., Fetterer, F., Windnagel, A. K. and Stewart., J. S.: *NOAA/NSIDC Climate Data Record of Passive Microwave Sea Ice Concentration, Version 4*. Southern Hemisphere, 1979-2020. Boulder, Colorado USA. NSIDC: National Snow and Ice Data Center. doi: https://doi.org/10.7265/efmz-2t65, 2021. Accessed June 3, 2023.

Meier, W. N., Windnagel, A., and Stewart, S.: CDR Climate Algorithm and Theoretical Basis Document: Sea Ice Concentration. NOAA NCEI CDR Program, 2021.

855   Mohrmann, M., Heuzé, C., and Swart, S.: Southern Ocean polynyas in CMIP6 models, The Cryo., 15, 4281–4313, https://doi.org/10.5194/tc-15-4281-2021, 2021.

Nakata, K., Ohshima, K. I., Nihashi, S., Kimura, N., and Tamura, T.: Variability and ice production budget in the Ross Ice Shelf Polynya based on a simplified polynya model and satellite observations, J. of Geophys. Res.: Oceans, 120, 6234–6252, 2015.

860 Nihashi, S. and Ohshima, K. J.: Circumpolar Mapping of Antarctic Coastal Polynyas and Landfast Sea Ice: Relationship and Variability, J. Clim, 28, 3650-3670, DOI: 10.1175/JCLI-D-14-00369.1, 2015.

Notz, D.: Sea-ice extent and its trend provide limited metrics of model performance. Cryo. 8, 229–243. (doi:10.5194/tc-8-229-2014), 2014.

Notz, D.: How well must climate models agree with observations?, Philosophical Transactions of the Royal Society of London

865 A: Mathematical, Phys. and Engin. Sci., 373, https://doi.org/10.1098/rsta.2014.0164, 2015.

Ohshima, K. I., Nihashi, S., and Iwamoto, K.: Global view of sea-ice production in polynyas and its linkage to dense/bottom water formation, Geoscience Letters, 3, 13, 2016.

O'Reilly, J. E., Maritorena, S., Mitchell, B. G., Siegel, D. A., Carder, K. L., Garver, S. A., Kahru, M. and McClain, C.: Ocean color chlorophyll algorithms for SeaWiFS, J. Geophys. Res., 103, 24,937– 24,953, 1998.

870 Parkinson, C. L. and Cavalieri, D. J.: Antarctic sea ice variability and trends, 1979–2010, The Cryo., 6, 871–880, https://doi.org/10.5194/tc-6-871-2012, 2012.

Parkinson, C., and Cavalieri, D.: Antarctic sea ice variability and trends, 1979–2010. *The Cryosphere*, **6**, 871–880, 2012.

Parkinson, C. L.: A 40-y record reveals gradual Antarctic sea ice increases followed by decreases at rates far exceeding the rates seen in the Arctic, P. Natl. Acad. Sci. USA, 116, 14414–14423, 2019.

875 Purich, A., and Doddridge, E. W.: Record low Antarctic sea ice coverage indicates a new sea ice state. Commun Earth Environ 4, 314. https://doi.org/10.1038/s43247-023-00961-9, 2023.

Raphael, M.N., and Handcock, M. S.: A new record minimum for Antarctic sea ice. Nat Rev Earth Environ 3, 215–216. https://doi.org/10.1038/s43017-022-00281-0, 2022.

Richert, I., Yager, P., Dinasquet, J., Logares, R., Riemann, L., Wendeberg, A., Bertilsson, S. and D. Scofield, D.: Summer

880 comes to the Southern Ocean: how phytoplankton shape bacterioplankton communities far into the deep dark sea. Ecosphere. 10. e02641. 10.1002/ecs2.2641, 2019.

Rodgers, K. B., Lee, S.-S., Rosenbloom, N., Timmermann, A., Danabasoglu, G., Deser, C., Edwards, J., Kim, J.-E., Simpson, I. R., Stein, K., Stuecker, M. F., Yamaguchi, R., Bódai, T., Chung, E.-S., Huang, L., Kim, W. M., Lamarque, J.-F., Lombardozzi, D. L., Wieder, W. R., and Yeager, S. G.: Ubiquity of human-induced changes in climate variability, Earth Syst.

885 Dynam., 12, 1393–1411, https://doi.org/10.5194/esd-12-1393-2021, 2021.

Singh, H. K. A. , Landrum, L., Holland, M. M., Bailey, D. A. and A. K. DuVivier, A. K.: An overview of Antarctic sea ice in the CESM2: analysis of the seasonal cycle, predictability, and atmosphere-ocean-ice interactions. J Adv Model Earth Syst., 13, https://doi.org/10.1029/2020MS002143, 2020.

Smith, A., Jahn, A., and Wang, M.: Seasonal transition dates can reveal biases in Arctic sea ice simulations, The Cryosphere,

890 14, 2977–2997, https://doi.org/10.5194/tc-14-2977-2020, 2020.

Smith, A., Jahn, A., Burgard, C., and Notz, D.: Improving model-satellite comparisons of sea ice melt onset with a satellite simulator, The Cryosphere, 16, 3235–3248, https://doi.org/10.5194/tc-16-3235-2022, 2022.

Stammerjohn, S. E., Martinson, D. G., Smith, R. C., Yuan, X. and Rind, D.: Trends in Antarctic annual sea ice retreat and advance and their relation to El Nin˜o–Southern Oscillation and Southern Annular Mode variability, J. Geophys. Res., 113, C03S90, doi:10.1029/2007JC004269, 2008.

Tamura, T., Ohshima, K. I., Enomoto, H., Tateyama, K., Muto, A., Ushio, S. and R. A. Massom, R. A.: Estimation of thin sea-ice thickness from NOAA AVHRR data in a polynya off the Wilkes Land coast, East Antarctica. Ann. Glaciol., 44, 269–274, 2006.

Tamura, T., Ohshima, K. I., Markus, T., Cavalieri, D. J., Nihashi, S. and N. Hirasawa, N.: Estimation of thin ice thickness and detection of fast ice from SSM/I data in the Antarctic Ocean, J. Atmos. Oceanic Technol., 24, 1757– 1772, 2007.

Tamura, T., Ohshima, K. I., and Nihashi, S.: Mapping of sea ice production for Antarctic coastal polynyas. Geophys Res Lett 35:L07606, 2008.

Tamura, T., Ohshima, K. I., Fraser, A. D. and G. D. Williams, G. D.: Sea ice production variability in Antarctic coastal polynyas, J. Geophys. Res. Oceans, 121, 2967–2979, doi:10.1002/2015JC011537, 2016.

Thompson, L., Smith, M., Thomson, J., Stammerjohn, S., Ackley, S., and Loose, B.: Frazil ice growth and production during katabatic wind events in the Ross Sea, Antarctica, The Cryosphere, 14, 3329–3347, https://doi.org/10.5194/tc-14-3329-2020, 2020.

Tsujino, H., Urakawa, S., Nakano, H., Small, R. J., Kim, W. M., Yeager, S. G., Danabasoglu, G., Suzuki, T., Bamber, J. L., Bentsen, M., B¨oning, C. W., Bozec, A., Chassignet, E. P., Curchitser, E., Boeira Dias, F., Durack, P. J., Griffies, S. M., Harada, Y., Ilicak, M., Josey, S. A., Kobayashi, C., Kobayashi, S., Komuro, Y., Large, W. G., Le Sommer, J., Marsland, S. J., Masina, S., Scheinert, M., Tomita, H., Valdivieso, M., and Yamazaki, D.: Jra-55 based surface dataset for driving ocean–sea-ice models (jra55-do). Ocean Modelling, **130**:79–139, 2018.

Turner, J., Phillips, T., Marshall, G. J., Hosking, J. S., Pope, J. O., Bracegirdle, T. J., and Deb, P.: Unprecedented springtime retreat of Antarctic sea ice in 2016, Geophys. Res. Lett., 44, 6868–6875, 2017.

Turner, J., Holmes, C., Caton Harrison, T., Phillips, T., Jena, B., Reeves-Francois, T., Fogt, R., Thomas, E. R., and Bajish, C. C.: Record low Antarctic sea ice cover in February 2022. Geophys. Res. Lett., 49, e2022GL098904, 2022.

Windnagel, A., Meier, W., Stewart, S., Fetterer, F., & Stafford, T.: NOAA/NSIDC Climate Data Record of Passive Microwave Sea Ice Concentration Version 4 Analysis. NSIDC Special Report 20. Boulder CO, USA: National Snow and Ice Data Center, 2021.

Zygmuntowska, M., Rampal, P., Ivanova, N. and L. H. Smedsrud, L. H.: Uncertainties in Arctic sea ice thickness and volume: new estimates and implications for trends, The Cryosphere, 8 (2), 705–720, doi:10.5194/tc-8-705-2014, 2014.